2.0
Axial-Flow Compressors

Meherwan P. Boyce

2121 Kirby Drive, Number 28N
Houston, TX 77019

713-807--0888
713-807-0088 Fax
boycepower.com
mpboyce@boycepower.com

2.0-1 Introduction

The compressors in most gas turbine applications, especially units over 5MW, use axial flow compressors. An axial flow compressor is one in which the flow enters the compressor in an axial direction (parallel with the axis of rotation), and exits from the gas turbine, also in an axial direction. The axial-flow compressor compresses its working fluid by first accelerating the fluid and then diffusing it to obtain a pressure increase. The fluid is accelerated by a row of rotating airfoils (blades) called the rotor, and then diffused in a row of stationary blades (the stator). The diffusion in the stator converts the velocity increase gained in the rotor to a pressure increase. A compressor consists of several stages: 1) A combination of a rotor followed by a stator make-up a stage in a compressor; 2) An additional row of stationary blades are frequently used at the compressor inlet and are known as Inlet Guide Vanes (IGV) to ensue that air enters the first-stage rotors at the desired flow angle, these vanes are also pitch variable thus can be adjusted to the varying flow requirements of the engine; and 3) In addition to the stators, another diffuser at the exit of the compressor consisting of another set of vanes further diffuses the fluid and controls its velocity entering the combustors and is often known as the Exit Guide Vanes (EGV).

In an axial flow compressor, air passes from one stage to the next, each stage raising the pressure slightly. By producing low-pressure increases on the order of 1.1:1 to 1.4:1, very high efficiencies can be obtained as seen in table 1. The use of multiple stages permits overall pressure increases of up to 40:1 in some aerospace applications and a pressure ratio of 30:1 in some Industrial applications.

The last twenty years has seen a large growth in gas turbine technology. The growth is spear headed by the increase in compressor pressure ratio, advanced combustion techniques, the growth of materials technology, new coatings and new cooling schemes. The increase in gas turbine efficiency is dependent on two basic parameters:

1. Increase in Pressure Ratio
2. Increase in Firing Temperature

It also should be remembered that the Gas Turbine Axial Flow Compressor consumes between 55%-65% of the power produced by the Turbine section of the gas turbine.

Table 1 Axial Flow Compressor Characteristics

Type of Application	Type of Flow	Inlet Relative Velocity Mach Number	Pressure Ratio per Stage	Efficiency per Stage
Industrial	Subsonic	0.4-0.8	1.05-1.2	88%-92%
Aerospace	Transonic	0.7-1.1	1.15-1.6	80%-85%
Research	Supersonic	1.05-2.5	1.8-2.2	75%-85%

The aerospace engines have been the leaders in most of the technology in the gas turbine. The design criteria for these engines was high reliability, high performance, with many starts and flexible operation throughout the flight envelope. The engine life of about 3500 hours between major overhauls was considered good. The aerospace engine performance has always been rated primarily on its Thrust/Weight ratio. Increase in engine Thrust / Weight Ratio is achieved by the development of high aspect ratio blades in the compressor as well as optimizing the pressure ratio and firing temperature of the turbine for maximum work output per unit flow.
The Industrial Gas Turbine has always emphasized long life and this conservative approach has resulted in the Industrial Gas Turbine in many

aspects giving up high performance for rugged operation. The Industrial Gas Turbine has been conservative in the pressure ratio and the firing temperatures. This has all changed in the last ten years; spurred on by the introduction of the "Aero-Derivative Gas Turbine" the Industrial Gas Turbine has dramatically improved its performance in all operational aspects. This has resulted in dramatically reducing the performance gap between these two types of gas turbines.

Figure 1 indicates the growth of the Pressure Ratio in a gas turbine over the past 50 years. The growth of both the Pressure Ratio and Firing Temperature parallel each other, as both growths are necessary to achieving the increase in thermal efficiency in Gas Turbines. The Axial flow compressor in most of the advanced gas turbine is a multistage compressor consisting of 17-22 stages with an exceedingly high pressure ratio. It is not uncommon to have pressure ratios in industrial gas turbines in the 17 to 20:1 range with some units having pressure ratios in the 30:1 range. Figure 2 shows a multistage high-pressure axial flow compressor rotor. The low-pressure increase per stage also simplifies calculations in the preliminary design of the compressor by justifying the air as incompressible in its flow through the stage.

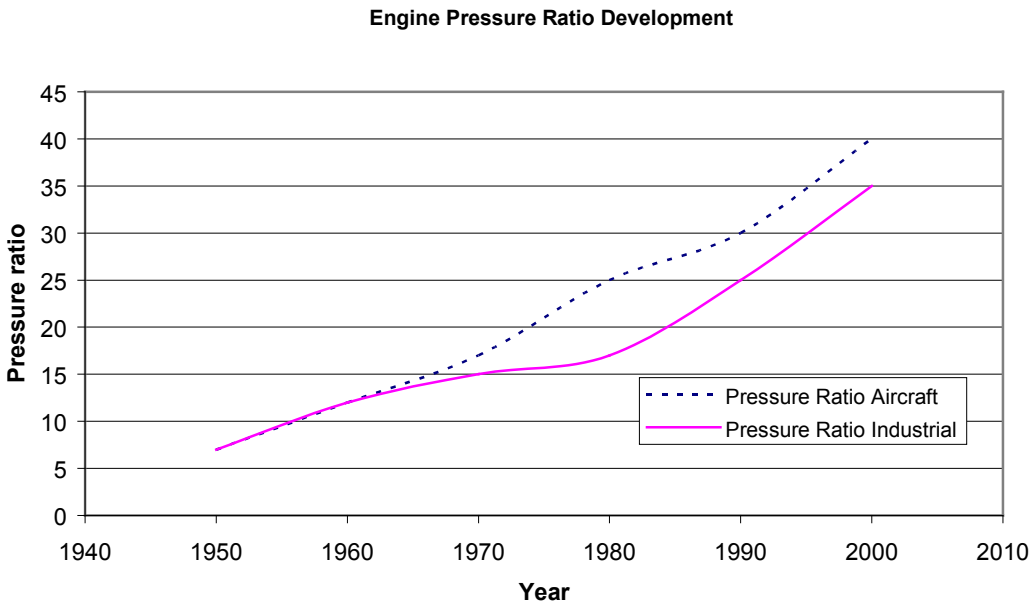

Fig.1.Development of pressure ratio over the past 50 years

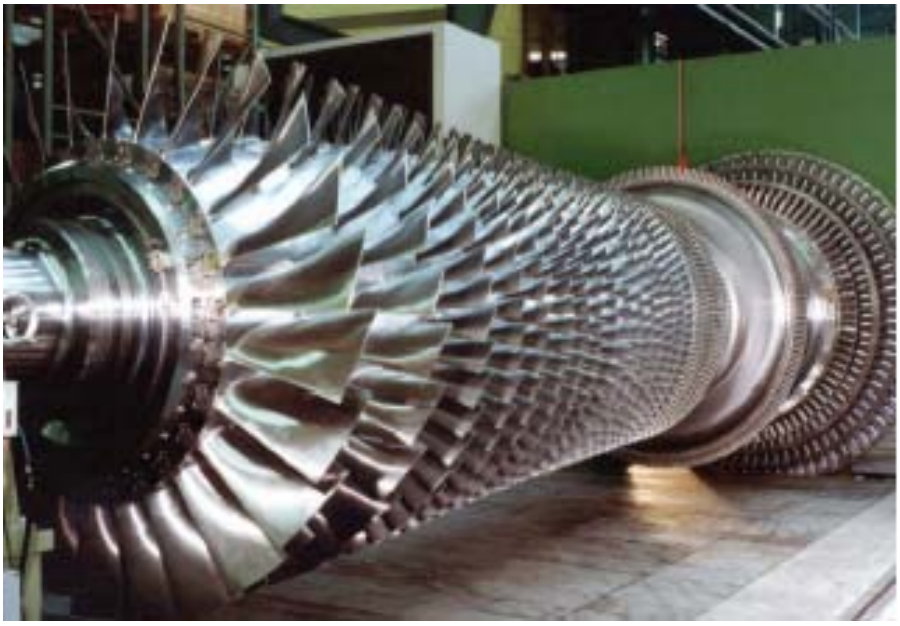

Fig. 2. Axial Flow Compressor Rotor

Figure 3 shows the stators, the stationary blades which are in between each rotor blade and causes the flow to be diffused (increase in the static pressure, reduction of the absolute velocity). The early stages of the stators in figure 3 are adjustable, as can be noted by their circular base. The adjustable stators allow the stator to be positioned to the correct flow angle leaving the blades as the air mass flow varies with load and inlet temperature.

Fig. 3. Axial Flow Compressor Stators located in the casing

As with other types of rotating machinery, an axial compressor can be described in a cylindrical coordinate system. The *z* axis is along the axis of rotation which is along the running length of the compressor shaft, the radius *r* is measured outward from the shaft, and the angle of rotation θ is the angle turned by the blades in figure 4. This coordinate system will be used throughout this discussion of axial-flow compressors.

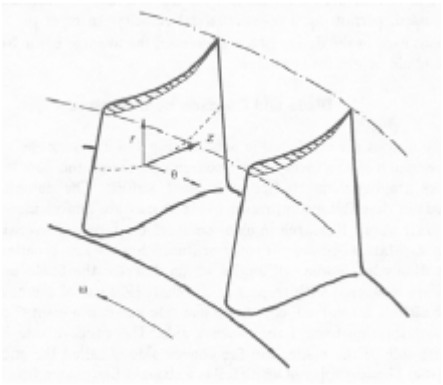

Fig. 4. Coordinate System for Axial-Flow Compressor

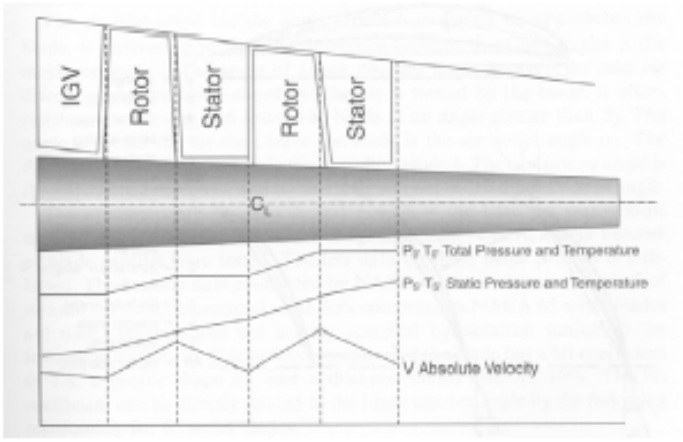

Fig. 5 Variation of Temperature Velocity, and Pressure through an Axial-Flow Compressor

Figure 5 shows the pressure, velocity, and total temperature variation for flow through several stages of an axial compressor. As indicated earlier in figure 3, the length of the blades, and the annulus area, this is the area between the shaft and shroud, decreases throughout the length of the compressor. This reduction in flow area compensates for the increase in fluid density as it is compressed, permitting a constant axial velocity. In most preliminary calculations used in the design of a compressor, the average blade height is used as the blade height for the stage.

2.0-2 Blade and Cascade Nomenclature

Since airfoils are employed in accelerating and diffusing the air in a compressor, much of the theory and research concerning the flow in axial compressors are based on studies of isolated airfoils. The nomenclature and methods of describing compressor blade shapes are almost identical to that of aircraft wings. Research in axial compressors involves the inter effect of one blade on the other; thus, several blades are placed in a row to simulate a compressor rotor or stator. Such a row is called a cascade. When discussing blades, all angles which describe the blade and its orientation are measured with respect to the shaft (Z axis) of the compressor.

The airfoils are curved, convex on one side and concave on the other, with the rotor rotating toward the concave side. The concave side is called the pressure side of the blade, and the convex side is called the suction side of the blade. The chordline of an airfoil is a straight line drawn from the leading edge to the trailing edge of the airfoil, and the chord is the length of the chordline as seen in figure 6. The camberline is a line drawn halfway between the two surfaces, and the distance between the camberline and the chordline is the camber of the blade. The camber angle θ is the turning angle of the camber line. The blade shape is described by specifying the ratio of the chord to the camber at some particular length on the chordline, measured from the leading edge. The aspect ratio *AR* is the ratio of the blade length to the chord length. The term "hub-to-tip ratio" is frequently used instead of aspect ratio. The aspect ratio becomes important when three-dimensional flow characteristics are discussed. The aspect ratio is established when the mass flow characteristics are discussed. The aspect ratio is established when the mass flow and axial velocity have been determined.

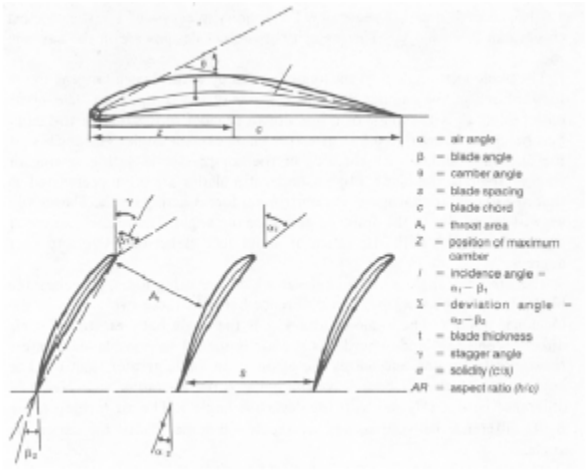

Fig. 6. Blade profile nomenclature

The pitch S_b of a cascade is the distance between blades, usually measured between the camberlines at the leading or trailing edges of the blades. The ratio of the chord length to the pitch is the solidity σ of the cascade. The solidity measures the relative interference effects of one blade with another. If the solidity is on the order of 0.5-0.7, the single or isolated airfoil test data, from which there are a profusion of shapes to choose, can be applied with considerable accuracy. The same methods can be applied up to a solidity of about 1.0 but with reduced accuracy. When the solidity is on the order of 1.0-1.5, cascade data are necessary. For solidity in excess of 1.5, the channel theory can be employed. The majority of present designs are in the cascade region.

The blade inlet angle β_1 is the angle formed by a line drawn tangent to the forward end of the camber line and the axis of the compressor. The blade outlet angle β_2 is the angle of a line drawn tangent to the rear of the camberline. Subtracting β_2 from β_1 gives the blade camber angle. The angle that the chordline makes with the axis of the compressor is γ, the setting or stagger angle of the blade. High-aspect ratio blades are often pretwisted so that at full operational speed the centrifugal forces acting on the blades will untwist the blades to the designed aerodynamic angle. The pretwist angle at the tip for blades with *AR* ratios of about four is between two and four degrees.

The air inlet angle α_1, the angle at which incoming air approaches the blade, is different from β_1. The difference between these two angles is the incidence angle *i*. The angle of attack α is the angle between the inlet air direction and the blade chord. As the air is turned by the blade, it offers resistance to turning and leaves the blade at an angle greater than β_2. The angle at which the air does leave the blade is the air outlet angle α_2. The difference between β_2 and α_2 is the deviation angle δ. The air turning angle is the difference between α_1 and α_2 and is sometimes called the deflection angle.

The original work by NACA and NASA is the basis on which most modern axial-flow compressors are designed. Under NACA, a large number of blade profiles were tested. The test data on these blade profiles is published. The cascade data conducted by NACA is the most extensive work on its kind. In most commercial axial-flow compressors in Gas Turbines built before 1990, NACA 65 series blades are used. These blades are usually specified by notation similar to the following: 65-(18) 10. This notation means that the blade has a lift coefficient of 1.8, a profile shape 65, and a thickness/chord ratio of ten percent (10%). The lift coefficient can be directly related to the blade camber angle by the following relationship for 65 series blades:

$$\Theta \approx 25\, C_{L_i} \qquad (1)$$

The new advanced compressor rotors have fewer blades with higher loadings, and the blades are thinner, larger, and are designed using advanced radial equilibrium theory, which create Three Dimensional and Controlled Diffusion shaped airfoils (3D/CDA), with smaller clearances and higher loading per stage.

2.0-3 Elementary Airfoil Theory

When a single airfoil is parallel to the velocity of a flowing gas, the air flows over the airfoil as shown in figure 7a. The air divides around the body, separates at the leading edge, and joins again at the trailing edge of the body. The main stream itself suffers no permanent deflection from the presence of the airfoil. Forces are applied to the foil by the local distribution of the steam and the friction of the fluid on the surface. If the airfoil is well designed, the flow is streamlined with little or no turbulence.

If the airfoil is set at the angle of attack to the air stream, as in figure 7b, a greater disturbance is created by its presence, and the streamline pattern will change. The air undergoes a local deflection, though at some distance ahead of and behind the body the flow is still parallel and uniform. The upstream disturbance is minor compared to the downstream disturbance. The local deflection of the air stream can, by Newton's laws, be created only if the blade exerts a force on the air; thus, the reaction of the air must produce an equal and opposite force on the airfoil. The presence of the airfoil has changed the local pressure distribution and, by the Bernoulli equation, the local velocities. Examination of the streamlines about the body shows that over the top of the airfoil, the lines approach each other, indicating an increase of velocity and a reduction in static pressure. On the underside of the airfoil, the action separates the streamlines, resulting in a static pressure increase.

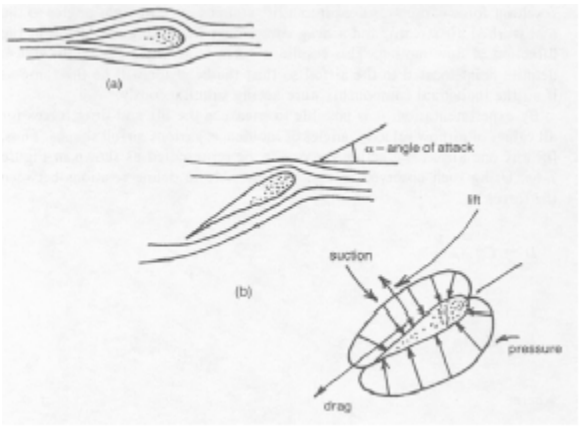

Fig. 7. Flow around an airfoil at various angles of attack:
a, parallel to the velocity of a flowing gas;
b, set at the angle of attack to the airstream;
c, pressure measurement at various points on airfoil's surface.

Measurement of the pressure at various points on the surface of the airfoil will reveal a pressure distribution as shown in figure 7c. The vectorial sum of these pressures will produce some resultant force acting on the blade. This resultant force can be resolved into a lift component *L* at right angles to the undisturbed air stream, and a drag component *D*, moving the airfoil in the direction of flow motion. This resultant force is assumed to act through a definite point located in the airfoil so that the behavior will be the same as if all the individual components were acting simultaneously.

By experimentation, it is possible to measure the lift and drag forces for all values of airflow velocity, angles of incidence, various airfoil shapes. Thus, for any one airfoil the acting forces can be represented as shown in figure 8a. Using such observed values, it is possible to define relations between the forces

$$D = C_D A \rho V^2/2 \quad (2)$$

$$L = C_L A \rho V^2/2 \quad (3)$$

where:

L = lift force
A = surface area
D = drag force
ρ = fluid density
C_L = lift coefficient
V = fluid velocity
C_D = drag coefficient

Two coefficients have been defined, C_L and C_D, relating velocity, density, area, and lift or drag forces. These coefficients can be calculated from wind-tunnel tests and plotted as shown in figure 8b versus the angle of attack for any desired section. These curves can then be employed in all future predictions involving this particular foil shape.

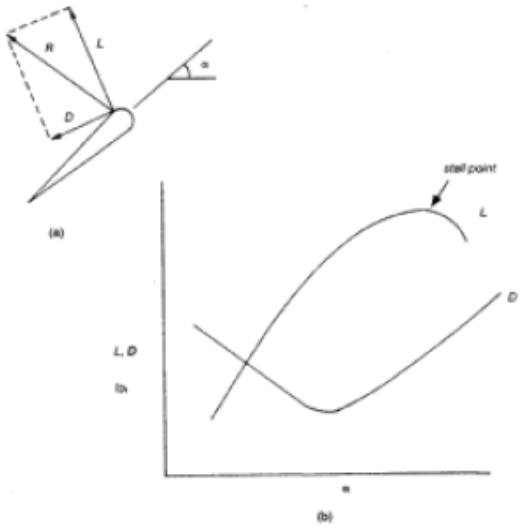

Fig. 8. Characteristics of the lift and drag forces on an airfoil

Examination of figure 8 reveals that there is an angle of attack which produces the highest lift force and lift coefficient. If this angle is exceeded, the airfoil "stalls" and the drag force increases rapidly. As this maximum angle is approached, a great percentage of the energy available is lost in overcoming friction, and a reduction in efficiency occurs. Thus, there is a point, usually before the maximum lift coefficient is reached, at which the most economical operation occurs as measured by effective lift for a given energy supply.

2.0-4 Laminar-Flow Airfoils

Just before and during World War II, much attention was given to laminar-flow airfoils. These airfoils are designed so that the lowest pressure on the surface occurs as far back as possible. The reason for this design is that the stability of the laminar boundary layer increases when the external flow is accelerated (in the flow with a pressure drop), and the stability decreases when the flow is directed against increasing pressure. A considerable reduction in skin friction is obtained by extending the laminar region in this way, provided that the surface is sufficiently smooth.

A disadvantage of this type of airfoil is that the transition from laminar to turbulent flow moves forward suddenly at small angles of attack. This sudden movement results in a narrow low-drag bucket, which means that the drag at moderate-to-large attack angles is much greater than an ordinary airfoil for the same attack angle as seen in figure 9. This phenomenon can be attributed to the minimum pressure point moving forward; therefore, the point of transition between laminar and turbulent flow is also advanced toward the nose as shown in figure 10. The more an airfoil is surrounded by turbulent airflow, the greater its skin friction will be.

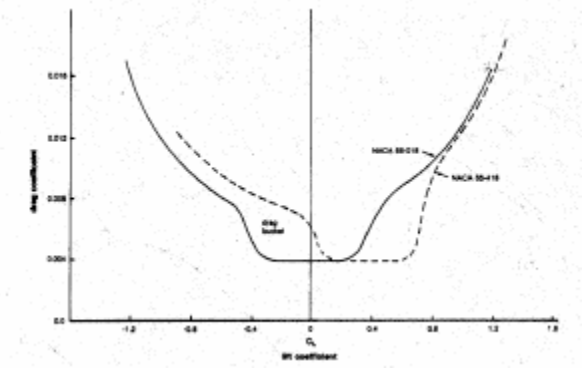

Fig. 9. NACA measurements of drag coefficients for two laminar airfoils

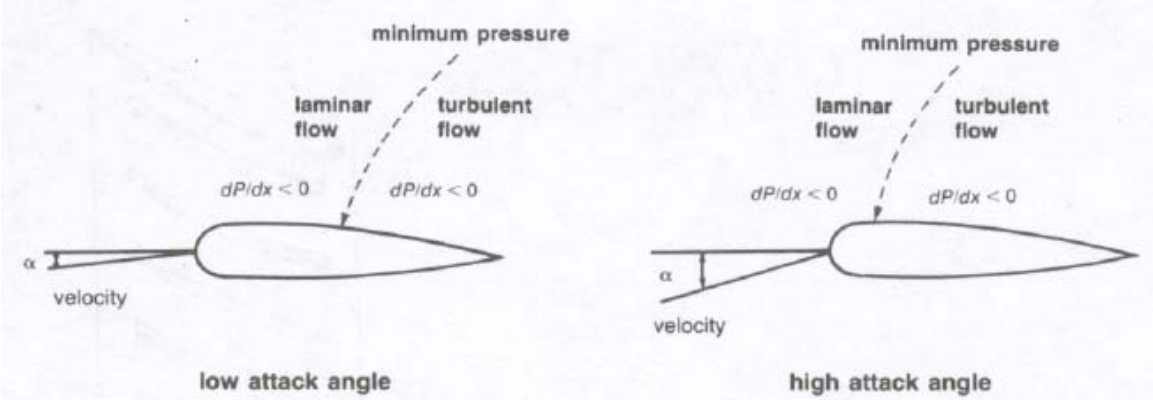

Fig 10. Laminar Flow Airfoils

2.0-5 Energy Increase

In an axial flow compressor, air passes from one stage to the next with each stage raising the pressure and temperature slightly. By producing low-pressure increases on the order of 1.1:1-1.4:1, very high efficiencies can be obtained. The use of multiple stages permits overall pressure increases up to 40:1. Figure 5 shows the pressure, velocity, and total temperature variation for flow through several stages of an axial flow compressor. It is important to note here that the changes in the total conditions for pressure, temperature, and enthalpy occur only in the rotating component where energy is inputted into the system. As seen also in figure 5, the length of the blades, and the annulus area, which is the area between the shaft and shroud, decrease throughout the length of the compressor. This reduction in flow area compensates for the increase in fluid density as it is compressed, permitting a constant axial velocity. In most preliminary calculations used in the design of a compressor, the average blade height is used as the blade height for the stage.

A heuristic approach for a multiple stage gas turbine compressor would be that the energy rise per stage would be constant, rather than the commonly held perception that the pressure rise per stage is constant. The energy rise per stage can be written as:

$$\Delta H = \frac{[H_2 - H_1]}{N_S} \tag{4}$$

where: H_1, H_2 = Total Inlet and Exit Enthalpy Btu/lb_m (kJ/kg) and

N_s = number of stages.

Assuming that the gas is thermally and caloricaly perfect (c_p, and γ are constant) equation 4 can be rewritten as:

$$\Delta T_{stage} = \frac{T_{in}\left[\left(\frac{P_2}{P_1}\right)^{\frac{\gamma-1}{\gamma}} - 1\right]}{N_s} \tag{5}$$

where: T_{in} = Total Inlet Temperature (ºF, ºC) and

P_1, P_2 = Total Inlet and Exit Pressure (psia, bar).

2.0-6 Velocity Triangles

As stated earlier, an axial-flow compressor operates on the principle of putting work into the incoming air by acceleration and diffusion. Air enters the rotor as shown in figure 11 with an absolute velocity (V) and an angle α_1, which combines vectorially with the tangential velocity of the blade (U) to produce the resultant relative velocity W_1 at an angle α_2. Air flowing through the passages formed by the rotor blades is given a relative velocity W_2 at an angle α_4, which is less than α_2 because of the camber of the blades. Note that W_2 is less than W_1, resulting from an increase in the passage width as the blades become thinner toward the trailing edges. Therefore, some

diffusion will take place in the rotor section of the stage. The combination of the relative exit velocity and blade velocity produce an absolute velocity V_2 at the exit of the rotor. The air then passes through the stator, where it is turned through an angle so that the air is directed into the rotor of the next stage with a minimum incidence angle. The air entering the rotor has an axial component at an absolute velocity V_{Z1} and a tangential component $V_{\theta 1}$.

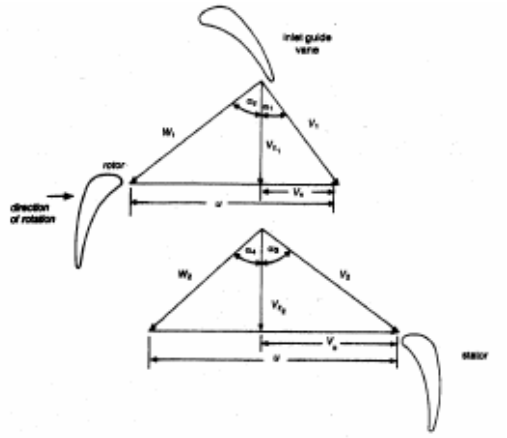

Fig. 11. Typical velocity triangles for an axial-flow compressor

Applying the Euler turbine equation

$$H = \frac{1}{g_c}\left[U_1 V_{\theta 1} - U_2 V_{\theta 2}\right] \tag{6}$$

and assuming that the blade speeds at the inlet and exit of the compressor are the same and noting the relationships,

$$V_{\theta 1} = V_{z1} \tan\alpha_1 \tag{7}$$

$$V_{\theta 2} = V_{z2} \tan\alpha_3 \tag{8}$$

Equation (1) can be written

$$H = \frac{U_1}{g_c}\left(V_{z1} \tan\alpha_2 - V_{z2} \tan\alpha_3\right) \tag{9}$$

Assuming that the axial component (V_Z) remains unchanged,

$$H = \frac{UV_z}{g_c}\left(\tan\alpha_1 - \tan\alpha_3\right). \tag{10}$$

The previous relationship is in terms of the absolute inlet and outlet velocities. By rewriting the previous equation in terms of the blade angles or the relative air angles, the following relationship is obtained:

$U_1 - U_2 = V_{Z1} \tan \alpha_1 = V_{Z1} \tan \alpha_2 = V_{Z2} \tan \alpha_3 + V_{Z2} \tan \alpha_4$.

Therefore,

$$H = \frac{UV_z}{g_c}\left(\tan\alpha_2 - \tan\alpha_4\right) \tag{11}$$

The previous relationship can be written to calculate the pressure rise in the stage:

$$c_p T_{in}\left[\left(\frac{P_2}{P_1}\right)^{\frac{\gamma-1}{\gamma}} - 1\right] = \frac{UV_2}{g_c}\left(\tan\alpha_2 - \tan\alpha_4\right) \tag{12}$$

which can be rewritten

$$\frac{P_2}{P_1} = \left\{\frac{UV_z}{g_c c_p T_{in}}\left[\tan\alpha_2 - \tan\alpha_4\right] + 1\right\}^{\frac{\gamma}{\gamma+1}}. \tag{13}$$

The velocity triangles can be joined together in several different ways to help visualize the changes in velocity. One of the methods is to simply join these triangles into a connected series. The two triangles can also be joined and superimposed using the sides formed by either the axial velocity, which is assumed to remain constant as shown in figure 12a, or the blade speed as a common side, assuming that the inlet and exit blade speed are the same as shown in figure 12b.

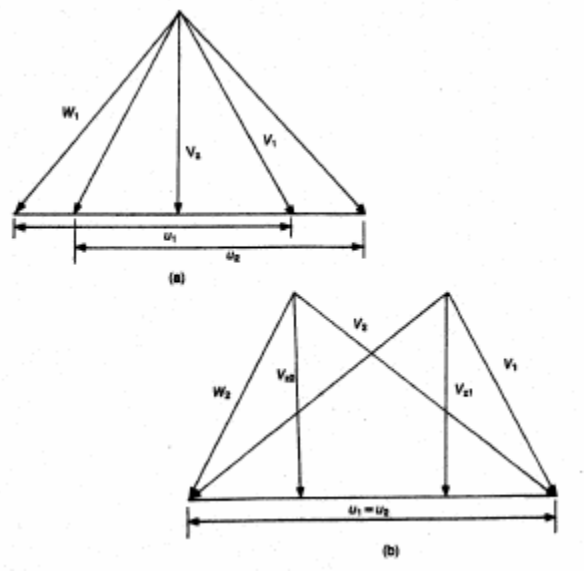

Fig. 12. Velocity triangles

2.0-7 Degree of Reaction

The degree of reaction in an axial-flow compressor is defined as the ratio of the change of static head in the rotor to the head generated in the stage:

$$R = \frac{H_{rotor}}{H_{stage}} \tag{14}$$

The change in static head in the rotor is equal to the change in relative kinetic energy:

$$H_r = \frac{1}{2g_c}\left(W_1^{\,2} - W_1^{\,2}\right) \tag{15}$$

and

$$W_1^{\,2} = V_{z1}^{\,2} + \left(V_{z1}\tan\alpha_2\right)^2 \tag{16}$$

$$W_2^{\,2} = V_{z2}^{\,2} + \left(V_{z2}\tan\alpha_4\right)^2 \tag{17}$$

Therefore,

$$H_r = \frac{V_z^{\,2}}{2g_c}\left(\tan^2\alpha_2 - \tan^2\alpha_4\right)$$

Thus, the reaction of the stage can be written

$$R = \frac{V_z}{2U}\,\frac{\tan^2\alpha_2 - \tan^2\alpha_4}{\tan\alpha_2 - \tan\alpha_4} \tag{18}$$

Simplifying the previous equation,

$$R = \frac{V_z}{2U}\left(\tan\alpha_2 + \tan\alpha_4\right) \tag{19}$$

In the symmetrical axial-flow stage, the blades and their orientation in the rotor and stator are reflected images of each other. Thus, in a symmetrical axial-flow stage where $V_1 = W_2$ and $V_2 = W_1$ as seen in figure 13, the head delivered in velocity as given by the Euler turbine equation can be expressed by the following relationships:

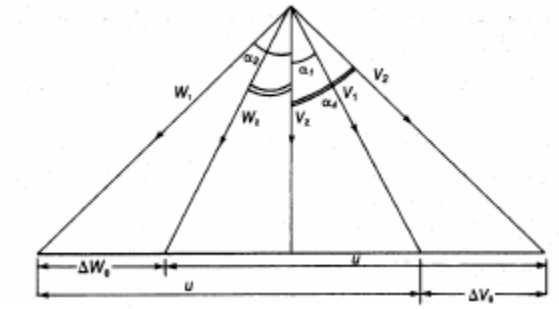

Fig. 13. Symmetrical velocity triangle for 50% reaction stage

$$H = \frac{1}{2g_c}\left[\left(U_1^2 - U_2^2\right) + \left(V_1^2 - V_2^2\right) + \left(W_2^2 - W_1^2\right)\right] \tag{20}$$

$$H = \frac{1}{2g_c}\left(W_2^2 - W_1^2\right) \quad . \tag{21}$$

The reaction for a symmetrical stage is fifty percent (50%). The fifty percent (50%) reaction stage is widely used, since an adverse pressure rise on either the rotor or stator blade surfaces is minimized for a given stage pressure rise. When designing a compressor with this type of blading, the first stage must be preceded by inlet guide vanes to provide prewhirl, and the correct velocity entrance angle to the first-stage rotor. With a high tangential velocity component maintained by each succeeding stationary row, the magnitude of W_1 is decreased. Thus, higher blade speeds and axial-velocity components are possible without exceeding the limiting value of 0.70-0.75 for the inlet Mach number. Higher blade speeds result in compressors of smaller diameter and less weight.

Another advantage of the symmetrical stage comes from the equality of static pressure rises in the stationary and moving blades, resulting in a maximum static pressure rise for the stage. Therefore, a given pressure ratio can be achieved with a minimum number of stages, a factor in the lightness of this type of compressor. The serious disadvantage of the symmetrical stage is the high exit loss resulting from the high axial velocity component. However, the advantages are of such importance in aircraft applications that the symmetrical compressor is normally used. In stationary applications, the symmetrical compressor is normally not used. In stationary applications, where weight and frontal area are of lesser importance, one of the other stage types is used.

The term “asymmetrical stage” is applied to stages with reaction other than 50%. The axial-inflow stage is a special case of an asymmetrical stage where the entering absolute velocity is in the axial direction. The moving blades impart whirl to the velocity of the leaving flow which is removed by the following stator. From this whirl and the velocity diagram as seen in figure 14, the major part of the stage pressure rise occurs in the moving row of blades with the degree of reaction varying from 60% to 90%. The stage is designed for constant energy transfer and axial velocity at all radii so that the vortex flow condition is maintained in the space between blade rows.

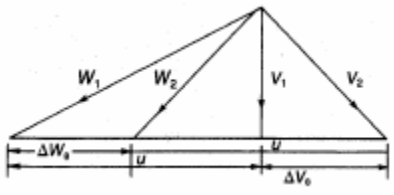

Fig. 14. Axial-entry stage velocity diagram

The advantage of a stage with greater than 50% reaction is the low exit loss resulting from lower axial velocity and blade speeds. Because of the small static pressure rise in the stationary blades, certain simplifications can be introduced such as constant-section stationary blades and the elimination of interstage seals. Higher actual efficiencies have been achieved in this stage type than with the symmetrical stage - primarily because of the reduced exit loss. The disadvantages result from a low static pressure rise in the stationary blades that necessitates a greater number of stages to achieve a given pressure ratio and thus creates a heavy compressor. The lower axial velocities and blade speed, necessary to keep within inlet Mach number limitations, result in large diameters. In stationary applications where the increased weight and frontal area are not of great importance, this type is frequently used to take advantage of the higher efficiency.

The axial-outflow stage diagram in figure 15 shows another special case of the asymmetrical stage with reaction greater than 50%. With this type of design, the absolute exit velocity is in an axial direction, and all the static pressure rise occurs in the rotor. A static pressure decrease occurs in the stator so that the degree of reaction is in excess of 100%. The advantages of this stage type are low axial velocity and blade speeds, resulting in the lowest possible exit loss. This design produces a heavy machine of many stages and of large diameter. To keep within the allowable limit of the inlet Mach number, extremely low values must be accepted for the blade velocity and axial velocity. The axial-outflow stage is capable of the highest actual efficiency because of the extremely low exit loss and the beneficial effects of designing for free vortex flow. This compressor type is particularly well-suited for closed-cycle plants where smaller quantities of air are introduced to the compressor at an elevated static pressure.

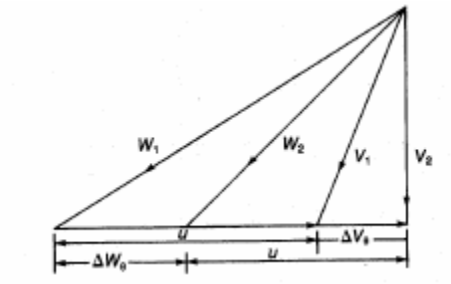

Fig. 15. Axial-outflow stage velocity diagram

While a reaction of less than 50% is possible, such a design results in high inlet Mach numbers to the stator row, causing high losses. The maximum total divergence of the stators should be limited to approximately 20° to avoid excessive turbulence. Combining the high inlet for the limiting divergence angles produces a long stator, thereby producing a longer compressor.

Radial Equilibrium

The flow in an axial-flow compressor is defined by the continuity, momentum, and energy equations. A complete solution to these equations is not possible because of the complexity of the flow in an axial-flow compressor. Considerable work has been done on the effects of radial flow in an axial-flow compressor. The first simplification used considers the flow axisymmetric. This simplification implies that the flow at each radial and axial station within the blade row can be represented by an average circumferential condition. Another simplification considers the radial component of the velocity as much smaller than the axial component velocity, so it can be neglected.

For the low-pressure compressor with a low-aspect ratio, and where the effect of streamline curvature is not significant, the simple radial equilibrium change of the radial velocity component along the axial direction is zero ($\partial V_{rad}/\partial_Z = 0$) and the change of entropy in the radial direction is zero negligible (a s/∂r = 0). The Meridional velocity (V_m) is equal to the axial velocity (V_Z), since the effect of steamline curvature is not significant. The radial gradient of the static pressure can be given

$$\frac{\partial P}{\partial r} = \rho \frac{V_\theta^2}{r} \quad . \tag{22}$$

Using the simple radial equilibrium equation, the computation of the axial velocity distribution can be calculated. The accuracy of the techniques depends on how linear V^2_θ/r is with the radius.

The assumption is valid for low-performance compressors, but it does not hold well for the high-aspect ratio, highly loaded stages where the effects of streamline curvature become significant. The radial acceleration of the Meridional velocity and the pressure gradient in the radial direction must be considered. The radial gradient of static pressure for the highly curved streamline can be written

$$\frac{\partial P}{\partial r} = \rho\left(\frac{V_\theta^2}{r} + \frac{Vm^2 \cos \in}{r_c}\right), \tag{23}$$

where $\in$ is the angle of the streamline curvature with respect to the axial direction and r_c is the radius of curvature.

To determine the radius of curvature and the streamline slope accurately, the configuration of the streamline through the blade row must be known. The streamline configuration is a function of the annular passage area, the camber and thickness distribution of the blade, and the flow angles at the inlet and outlet of the blade. Since there is no simple way to calculate the effects of all the parameters, the techniques used to evaluate these radial accelerations are empirical. By using iterative solutions, a relationship can be obtained. The effect of high radial acceleration with high-aspect ratios can be negated by tapering the tip of the compressor inward so that the hub curvature is reduced.

Diffusion Factor

The diffusion factor first defined by Lieblien is a blade-loading criterion:

$$D = \left(1 - \frac{W_2}{W_1}\right) + \frac{V_{\theta 1} - V_{\theta 2}}{2\sigma W_1}. \tag{24}$$

The diffusion factor should be less than 0.4 for the rotor tip and less than 0.6 for the rotor hub and the stator. The distribution of the diffusion factor throughout the compressor is not properly defined. However, the efficiency is less in the later stages due to distortions of the radial velocity distributions in the blade rows. Experimental results indicate that even though efficiency is less in the later stages, as long as the diffusion loading limits are not exceeded, the stage efficiencies remain relatively high.

The Incidence Rule

For low-speed airfoil design, the region of low-loss operation is generally flat, and it is difficult to establish the precise value of the incidence angle that corresponds to the minimum loss as seen in figure 16. Since the curves are generally symmetrical, the minimum loss location was established at the middle of the low-loss range. The range is defined as the change in incidence angle corresponding to a rise in the loss coefficient equal to the minimum value.

The following method for calculation of the incidence angle is applicable to cambered airfoils. Work by NASA on the various cascades is the basis for the technique. The incidence angle is a function of the blade camber, which is an indirect function of the air-turning angle.

$$i = ki_0 + m\varsigma + \delta_m \tag{25}$$

where i_0 is the incidence angle for zero camber, and m is the slope of the incidence angle variation with the air-turning angle (ξ). The zero-camber incidence angle is defined as a function of inlet air angle and solidity as seen in figure 17 and the value of m is given as a function of the inlet air angle and the solidity as seen in figure 18.

The incidence angle i_o is for a 10% blade thickness. For blades of other than 10% thickness, a correction factor K is used, which is obtained from figure 19.

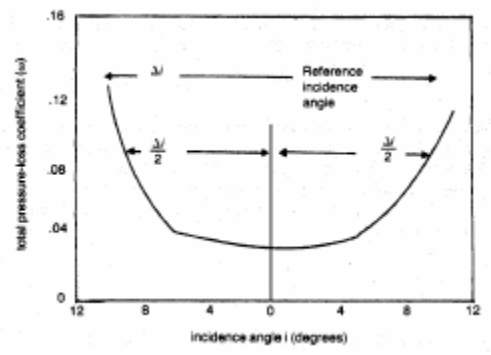

Fig. 16. Loss as a function of incidence angle

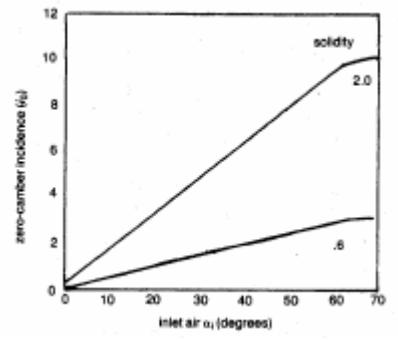

Fig. 17. Incidence angle for zero-camber airfoil

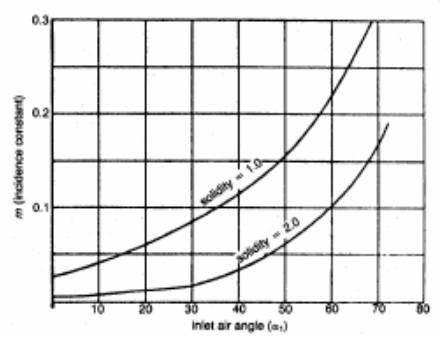

Fig 18. Slope of incidence angle variation with air angle

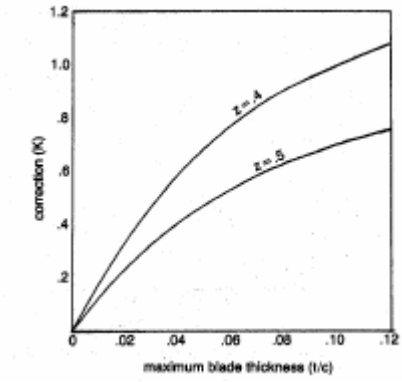

Fig. 19. Correction factor for blade thickness and incidence angle calculation

The incidence angle now must be corrected for the Mach number effect (δ_m). The effect of the Mach number on incidence angle is shown in figure 20. The incidence angle is not affected until a Mach in number of 0.7 is reached.

The incidence angle is now fully defined. Thus, when the inlet and outlet air angles and the inlet Mach number are known, the inlet blade angle can be computed in this manner.

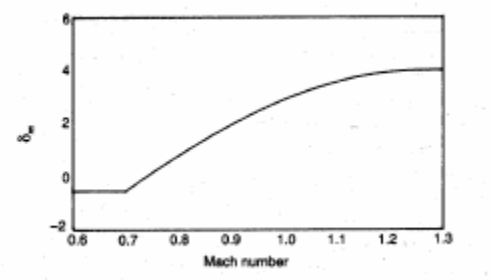

Fig. 20. Mach-number correction for incidence angle

2.0-8 The Deviation Rule

Carter's rule, which shows that the deviation angle is directly a function of the camber angle and is inversely proportional to the solidity $\left(\delta = m\theta\sqrt{1/\sigma}\right)$ has been modified (Boyce) to take into account the effect of stagger, solidity, Mach number, and blade shape as shown in the following relationship:

$$\delta_f = m_f\theta\sqrt{1/\sigma} + 12.15\,t/c\left(1-\theta/8.0\right) + 3.33\left(M_1 - 0.75\right) \tag{26}$$

where m_f is a function of the stagger angle, maximum thickness, and the position of maximum thickness as seen in figure 21. The second term of the equation should only be used for camber angles $0 < \theta > 8$. The third term must be used only when the mach number is between $0.75 < M > 1.3$.

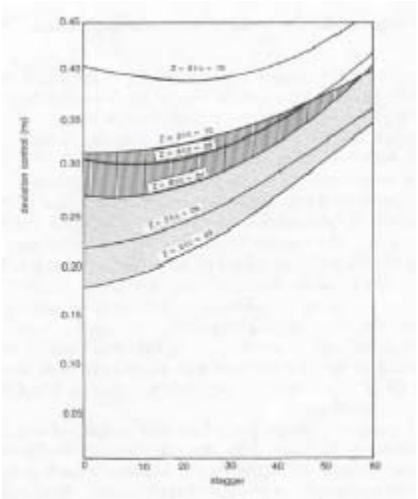

Fig. 21. Position of maximum thickness effect on deviation

The use of NACA cascade data for calculating the exit air angle is also widely used. Mellor has replotted some of the low-speed NACA 65 series cascade data in convenient graphs of inlet air angle against exit air angle for blade sections of given lift and solidity set at various staggers. Figure 22 shows the NACA 65 series of airfoils.

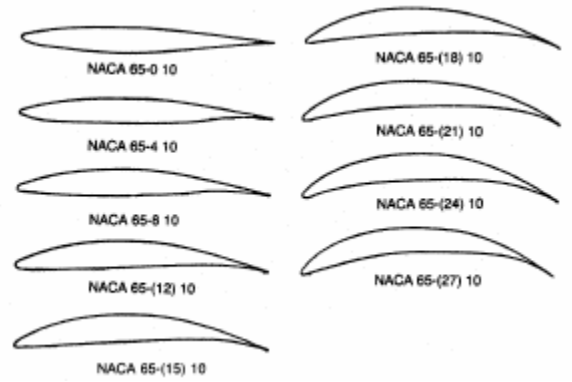

Fig. 22. The NACA 65 series of cascade airfoils

The 65 series blades are specified by an airfoil notation similar to 65-(18)10. This specification means that an airfoil has the profile shape 65 with a camber line corresponding to a life coefficient (C_L) = 1.8 and approximate thickness of 10% of the chord length. The relationship between the camber angle and the lift coefficient for the 65 series blades is shown in figure 23.

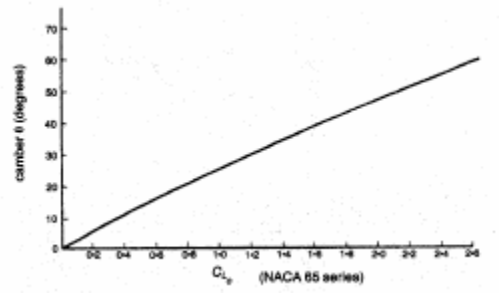

Fig. 23. Approximate relation between camber (θ) and C_{L0} of NACA 65 series

The low-speed cascade data have been replotted by Mellor in the form of graphs of α_2 against α_1 for blade sections of given camber and space-chord ratio but set at varying stagger γ, and tested at varying incidence ($i = \alpha_i - \beta_1$) or angle of attack ($\alpha_1 - \gamma$) as seen in figure 24. The range on each block of results is indicated with heavy black lines, which show the attack angle at which the drag coefficient increases by 50% over the mean unstalled drag coefficient.

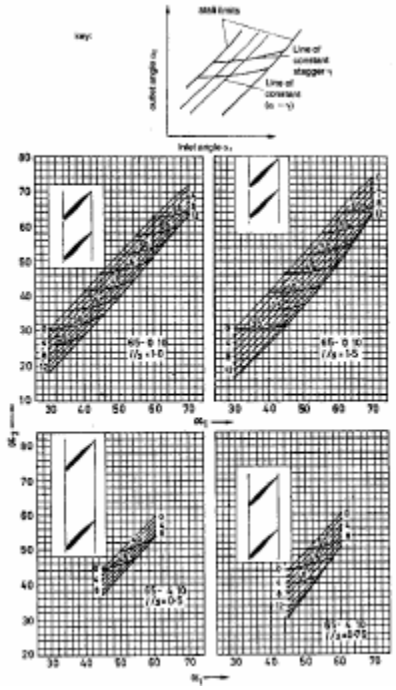

Fig. 24. The NACA 65 series cascade data
(Reprinted, by permission of G. Mellor, Massachusetts Institute of Technology, Gas Turbine Laboratory Publication.)

NACA has given “design points” for each cascade tested. Each design point is chosen on the basis of the smoothest pressure distribution observed on the blade surfaces: if the pressure distribution is smooth at one particular incidence at low speed, it is probable that the section will operate efficiently at a higher Mach number at the same incidence, and that this same incidence should be selected as a design point.

Although such a definition appears somewhat arbitrary at first, the plots of such design points against solidity and camber give consistent curves. These design points are replotted in figure 25, showing the angle of attack (α_1 - γ) plotted against space-chord ratio and camber is independent of stagger.

If the designer has complete freedom to choose space-chord ratio, camber, and stagger, then a "design point" choice may be made by trial and error from the plots of figure 24 and 25. For example, if an outlet angle (α_2) of 15 is required from an inlet angle of 35, a reference to the curves of the figures will show that a space-chord ratio of 1.0, camber 1.2, and stagger 23 will give a cascade operating at its design point. There is a limited variety of cascades of different space-chord ratios, but only one cascade that will operate at “design point” at the specified air angles. For example, if the space-chord ratio were required to be 1.0 in the previous example, then the only cascade that will produce design point operation is that of camber 1.2, stagger 23.

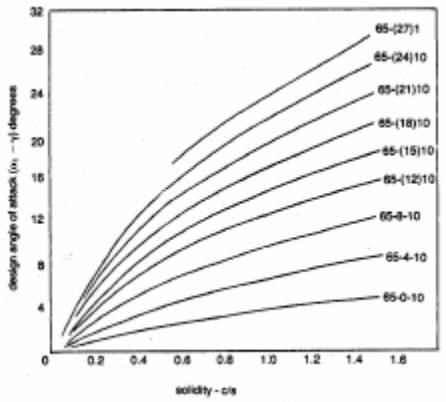

Fig 25. Design angles of attack (α_1 - γ) for NACA 65 series

Such a design procedure may not always be followed, for the designer may choose to design the stage to operate closer to the positive stalling limit or closer to the negative stalling (choking) limit at design operating conditions to obtain more flexibility at off-design conditions.

2.0-9 Compressor Operation Characteristics

A compressor operates over a large range of flow and speed delivering a stable head/pressure ratio. During start up the compressor must be designed to operate in a stable condition at low rotational speeds. There is an unstable limit of operation known as ‘surging’, and it is shown on the performance map as the surge line. The surge point in a compressor occurs when the compressor back pressure is high and the compressor can not pump against this high head causing the flow to separate and reverse its direction. Surge is a reversal of flow and is a complete breakdown of the continuous steady flow through the whole compressor. It results in mechanical damage to the compressor due to the large fluctuations of flow which results in changes in direction of the thrust forces on the rotor creating damage to the blades and the thrust bearings. The phenomenon of surging should not be confused with the stalling of a compressor stage. Stalling is the breakaway of the flow from the suction side of the blade aerofoil thus causing an aerodynamic stall. A multi-stage compressor may operate stably in the unsurged region with one or more of the stages stalled, and the rest of the stages unstalled.

Compressor Surge

Compressor surge is a phenomenon of considerable interest; yet, it is not fully understood. It is a form of unstable operation and should be avoided. It is a phenomenon that unfortunately occurs frequently, sometimes with damaging results. *Surge* has been traditionally defined as the lower limit of stable operation in a compressor, and it involves the reversal of flow. This reversal of flow occurs because of some kind of aerodynamic instability within the system. Usually, a part of the compressor is the cause of the aerodynamic instability, although it is possible for the system arrangement to be capable of augmenting this instability. Compressors are usually operated at a working line, separated by some safety margin from the surge line. Extensive investigations have been conducted on surge. Poor quantitative universality or aerodynamic loading capacities of different blades and stators, and an inexact knowledge of boundary-layer behavior make the exact prediction of flow in the compressor at the off-design stage difficult.

A decrease in the mass flow rate, an increase in the rotational speed of the impeller, or both can cause the compressor to surge. Whether surge is caused by a decrease in flow velocity or an increase in rotational speeds, the blades or the stators can stall. One should note that operating at higher efficiency implies operation closer to surge. It should be noted here that total pressure increases occur only in the rotational part of the compressor, the blades. To make the curve general, the concept of aerodynamic speeds and corrected mass flow rates has been used in the performance maps in this chapter.

The surge line slope on multistage compressors can range from a simple single parabolic relationship to a complex curve containing several break-points or even "notches." The complexity of the surge line shape depends on whether or not the flow limiting stage changes with operating speed from one compression stage to another; in particular, very closely matched stage combinations frequently exhibit complex surge lines. In the case of compressors with variable inlet guide vanes, the surge line tends to bend more at higher flows than with units which are speed controlled.

Usually surge is linked with excessive vibration and an audible sound; yet, there have been cases where surge not accompanied by audible sound has caused failures. Usually, operation in surge and, often, near surge is accompanied by several indications, including general and pulsating noise level increases, axial shaft position changes, discharge temperature excursions, compressor differential pressure fluctuations, and lateral vibration amplitude increases. Frequently, with high pressure compressors, operation in the incipient surge range is accompanied by the emergence of a low frequency, asynchronous vibration signal which can reach predominant amplitudes, as well as excitation of various harmonics of blade passing frequencies. Extended operation in surge causes thrust and journal-bearing failures. Failures of blades and stators are also experienced due to axial movement of the shaft causing contact of blades and stators. Due to the large flow instabilities experienced severe aerodynamic stimulation at one of blade natural response frequencies is caused, leading to blade failure.

The performance map, of an axial flow compressors displays the variation of total pressure ratio across a compressor, as a function of corrected mass flow (usually expressed as percent of design value), at a series of constant corrected speed lines (N_c). The axial flow compressor adiabatic efficiency (η_c) is shown as islands on the performance map, and can also be depicted versus corrected mass flow and is shown for a representative multi-stage compressor in figure 26.

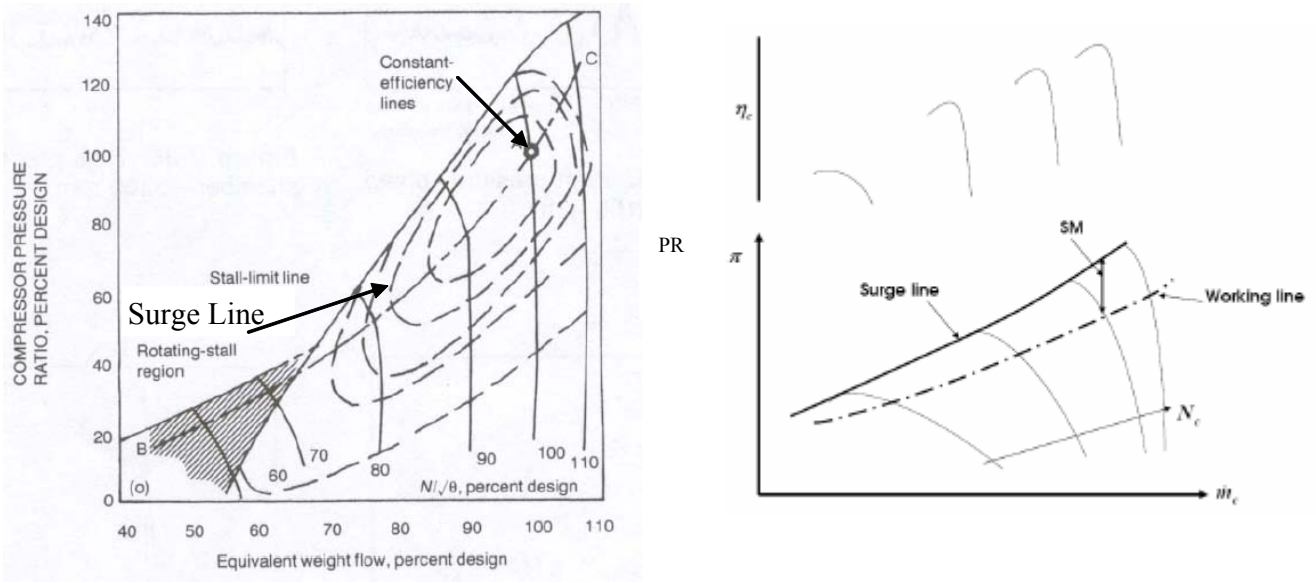

Fig. 26. Multi-Stage Axial Compressor Maps

On a given corrected speed line, as the corrected mass flow is reduced, the pressure ratio (usually) increases until it reaches a limiting value on the surge line. For an operating point at or near the surge line the "orderly" flow (i.e. nearly axisymmetric) in the compressor tends to "break" down (flow becomes asymmetric with rotating stall) and can become "violently" unsteady. Thus the surge line is a locus of unstable compressor operating points and is to be avoided. To cope with this, one specifies the surge margin *SM* defines as:

$$SM = \frac{(PR_{surge} - PR_{working})}{PR_{working}}. \qquad (27)$$

In Equation (27) $PR_{surge/working}$ denotes the pressure ratio on the surge/working line at the same corrected mass flow rate; thus the corrected speed would be higher for operating points on the surge line. For operation on a constant corrected speed line an alternative definition for surge margin in terms of corrected mass flow on the working line and on surge line at the same corrected speed would be preferable. For stable operation of a multi-stage compressor a surge margin is specified.

Compressors are designed to operate at a condition referred to as the *design point*. At the design point the various stages mounted on the same shaft are matched aerodynamically i.e. the inlet flow to each stage is such that the stage is at the design point and this occurs for only one combination of corrected speed and mass flow (for this reason the design point is also known as match point). While the design point is one at which the compressor will operate most of the time, there are situations of low-speed operation during the starting of gas turbines where the compressor must also provide adequate pressure rise and efficiency. For compressor operations

at corrected speed or at the same corrected speed but corrected mass flow different from those at design, difficulties arise due to the requirements of matching the inlet flow to one stage to the outlet flow from those upstream. As an illustration, consider changes along the constant corrected speed line. The effect of reduction in mass flow relative to the working line results in a higher pressure rise and therefore a greater increase in density in the first stage than was predicted at design. The greater increase in density means the second stage has an even lower value of flow coefficient than the first stage, with an even greater increase in density. The effect is cumulative, so that the last stage approaches stall while the front stage is only slightly altered. Conversely increasing the mass flow relative to the working line would result in a lower pressure rise and therefore a smaller increase in density. The smaller increase in density means the second stage has an even higher value of flow coefficient than the first stage, with an even smaller increase in density. The consequence is that the last stage approaches stalling at negative incidence with low efficiency performance. Similarly one can also show that reducing the rotational speed along the working line through the design point can lead to stalling of front stages and wind-milling of rear stages. Methods for coping with low-speed difficulties include use of compressor air bleed at the intermediate stage, use of variable geometry compressor, and use of multi-spool compressors or combinations of the above.

Compressor Choke

The compressor choke point is when the flow in the compressor reaches Mach 1 at the blade throat, a point where no more flow can pass through the compressor. This phenomenon is often known in the industry as “Stone Walling.” The more stages, the higher the pressure ratio, and the smaller the operational margin between surge and choke regions of the compressor as shown in figure 27.

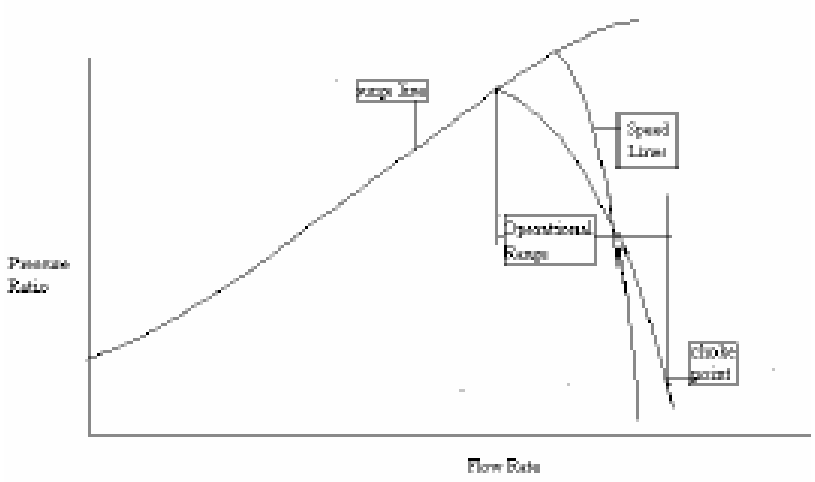

Fig. 27. A High Pressure Multistage Axial Flow compressor map

Compressor Stall

There are three distinct stall phenomena. Rotating stall and individual blade stall are aerodynamic phenomena; stall flutter is an aero elastic phenomenon.

Individual Blade Stall

This type of stall occurs when all the blades around the compressor annulus stall simultaneously without the occurrence of a stall propagation mechanism. The circumstances under which individual blade stall is established are unknown at present. It appears that the stalling of a blade row generally manifests itself in some type of propagating stall and that individual blade stall is an exception.

Rotating Stall

Rotating, or propagating stall, was first observed by Whittle and his team on the inducer vanes of a centrifugal compressor. Rotating stall (propagating stall) consists of large stall zones covering several blade passages and propagates in the direction of the rotation and at some fraction of rotor speed. The number of stall zones and the propagating rates vary considerably. Rotating stall is the most prevalent type of stall phenomenon.

The propagation mechanism can be described by considering the blade row to be a cascade of blades as shown in figure 28. A flow perturbation causes blade 2 to reach a stalled condition before the other blades. This stalled blade does not produce a sufficient pressure rise to maintain the flow around it, and an effective flow blockage or a zone of reduced flow develops. This retarded flow diverts the flow around it so that the angle of attack increases on blade 3 and decreases on blade 1. In this way a stall ‘cell’ may move

along the cascade in the direction of the lift on the blades. The stall propagates downward relative to the blade row at a rate about half the rotational speed; the diverted flow stalls the blades below the retarded-flow zone and unstalls the blades above it. The retarded flow or stall zone moves from the pressure side to the suction side of each blade in the opposite direction of rotor rotation. The stall zone may cover several blade passages. The relative speed of propagation has been observed from compressor tests to be less than the rotor speed. Observed from an absolute frame of reference, the stall zones appear to be moving in the direction of rotor rotation. The radial extent of the stall zone may vary from just the tip to the whole blade length. Table 2 shows the characteristics of rotating stall for single and multistage axial-flow compressors.

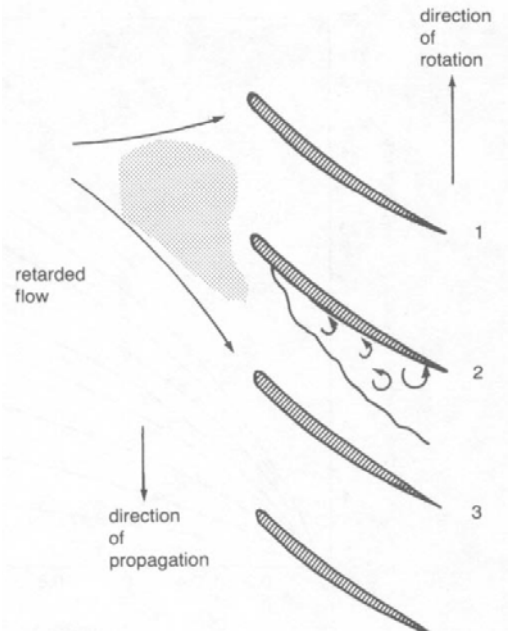

Fig. 28. Propagating Stall in a Blade Cascade

Table 2 Summary of Rotating Stall Data

Single-Stage Compressors						
Type of Velocity Diagram	**Hub-tip Radius Ratio**	**Number of Stall Zones**	**Propagation Rate, Stall Speed, abs/ Rotor Speed**	**Weight-flow Fluctuation during stall,** $\Delta\left(\frac{PV}{PV}\right)$	**Radial Extent of Stall Zone**	**Type of Stall**
Symmetrical	0.50	3	0.420	1.39	Partial	Progressive
		4	0.475	2.14	↓	↓
		5	0.523	1.66		
	0.90	1	0.305	1.2	Total	Abrupt
	0.80	8	0.87	0.76	Partial	Progressive
		1	0.36	1.30	Total	Abrupt
	0.76	7	0.25	2.14	Partial	Progressive
		8	0.25	1.10	↓	↓
		5	0.25	1.10	↓	↓
		3	0.23	2.02		
		4	0.48	1.47	Total	
		3	0.48	2.02	↓	
		2	0.49	1.71	↓	
	0.72	6, 8	0.245	0.71=1.33	Total	Progressive
Free	0.60	1	0.48	0.60	Partial	Progressive
vortex		2	0.36	0.60	Partial	Progressive
		1	0.10	0.68	Total	Abrupt
Solid	0.60	1	0.45	0.60	Partial	Progressive
body		1	0.12	0.65	Total	Abrupt
Vortex	0.50	3	0.816		Partial	Progressive
transonic		2	0.634		Total	Progressive
	0.50	1	0.565		Total	Abrupt
	0.40	2			Partial	Progressive

Multistage Compressors						
Type of Velocity Diagram	**Hub to Tip Ratio**	**Number of Stall Zones**	**Propagation Rate, Stall Speed, abs/Rotor Speed**	**Radial Extent of Stall Zone**	**Periodicity**	**Type of Stall**
Symmetrical	0.5	3	0.57	Partial	Steady	Progressive[1]
		4	↓	↓	↓	↓
		5				
		6				
		7				
Symmetrical	0.9	4	0.55	Partial	Intermittent	Progressive
		5	↓	↓	↓	↓
		6				
Symmetrical	0.80	1	0.48	Partial	Steady	Progressive
Symmetrical	0.76	1	0.57	Partial	Steady	Progressive
		2	↓			
		3		↓	↓	↓
		4				
Symmetrical	0.72	1	0.57	Partial	Intermittent	Progressive
		2				
		3	↓	↓	↓	↓
		4				
		5				
Free Vortex	0.60	1	0.47	Total	Steady	Abrupt[2]
Solid Body	0.60	1	0.43	Total	Steady	Abrupt
Vortex Transonic	0.50	1	0.53	Total	Steady	Abrupt

[1]Progressive Stall indicates the gradual increase in blocked annulus area due to stall.
[2]Abrupt Stall is a single stall zone covering as much as half the annulus area and extending over the entire blade span with discontinuity in the pressure curve. Complete Compressor Stall is applied to multistage compressors to describe a discontinuous performance curve similar to that for abrupt stall, and these points define the stall-limit line.

Stall Flutter

This phenomenon is caused by self-excitation of the blade and is an aero-elastic phenomenon. It must be distinguished from classic flutter, since classic flutter is a coupled torsional-flexural vibration that occurs when the free-stream velocity over a wing or airfoil section reaches a certain critical velocity. Stall flutter, on the other hand, is a phenomenon that occurs due to the stalling of the flow around a blade.

Blade stall causes Karman vortices in the airfoil wake. Whenever the frequency of these vortices coincides with the natural frequency of the airfoil, flutter will occur. Stall flutter is a major cause of compressor blade failure.

Several types of flutter have been identified and these are indicated as various flutter boundaries on the operating map of a high-speed (transonic) compressor in figure 29. Besides $\dot{m}_c$ and N_c, additional non-dimensional parameters have to be introduced to adequately characterize the flutter boundaries. One such parameter is the reduced frequency which is given by the ratio of blade chord to the wavelength of the unsteady disturbance induced by the blade motion. Often the inverse of reduced frequency, the reduced velocity is used instead. More recently Khalak (2002) proposed and developed a framework for flutter operability assessment in which a set of four non-dimensional parameters is used to characterize the flutter boundary. These parameters are the corrected mass flow, the corrected speed, the compressible reduced frequency $\left(\frac{c\,\omega_0}{\sqrt{\gamma RT}}\right)$ (where c denotes blade chord length, ω_0 the modal frequency) and the combined mass-damping parameter (ratio of mechanical damping to blade mass). In analogy with the surge margin, a flutter margin FM is specified in equation (28):

$$FM = \frac{(PR_{flutter} - PR_{working})}{PR_{working}} \quad (28)$$

$PR_{flutter}$ is the pressure ratio on the flutter boundary at the same corrected mass flow corresponding to that for $PR_{working}$ on the working line. For operation on a constant corrected speed line, it would be preferable to define flutter margin in terms of corrected mass flow on the working line and on the flutter boundary at the same corrected speed.

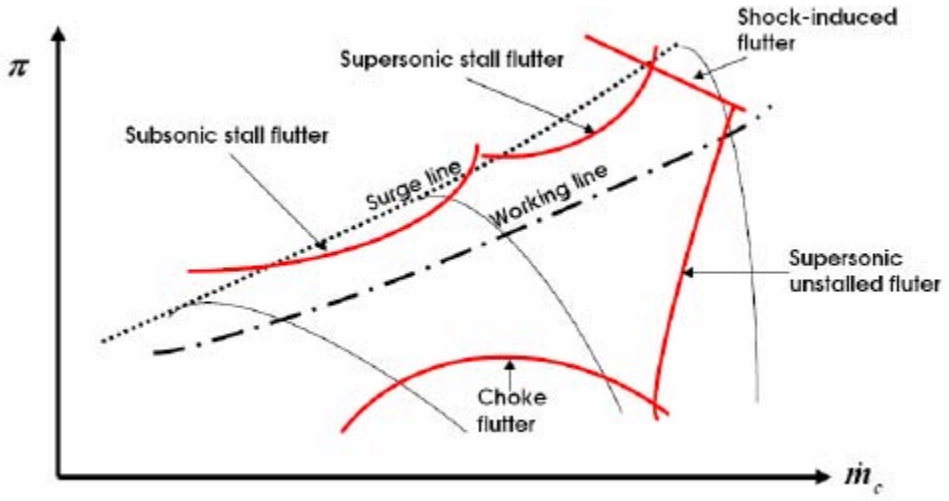

Fig. 29. Flutter regions on the operating map of a transonic compressor (after Mikolajczak, et al., 1975)

An example of a typical failure due to flutter in an axial flow compressor fifth stage is discussed in this section. There were three blade failures of the fifth stage blade all within 3-10 hours of operation. The cause of the failure had to be determined. A dynamic pressure transducer with a voltage output was used to obtain the frequency spectra. In the first four stages of the compressor no outstanding vibration amplitudes were recorded. A signal was noted at 48*N* (*N* being the running speed), but the amplitude was not high, and it did not fluctuate. A measurement at the low-pressure bleed chamber taken from the fourth stage showed similar characteristics. The compressor high-pressure bleed chamber occurs after the eighth stage. A measurement at this chamber showed a high, fluctuating 48*N* signal. As there are 48 blades on the fifth-stage wheel, a problem in the fifth-stage was suspected. However, above the fifth-stage are blade rows of 86*N* (2 x 48*N*), so further analysis was needed. It was found that the measurement at the high-pressure bleed chamber showed only a very small 86*N* amplitude compared to the high amplitude of the 48*N* frequency. Since blade rows of 86 blades were closer to the high-pressure bleed chamber, the expected high signal should have been 86*N* compared to 48*N* under normal operating conditions. This high amplitude of 48*N* indicated that it was the fifth-stage which caused the high, fluctuating signal; thus, a stall condition in that section was probable.

Figures 30, 31, 32, and 33 show the spectrum at speeds of 4,100; 5,400; 8,000; and 9,400 rpm. At 9,400 rpm, the second and third harmonics of 48*N* were also very predominant.

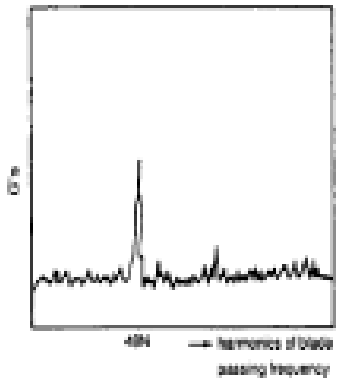

Fig. 30. High-Pressure Bleed Chamber - 4,100 rpm

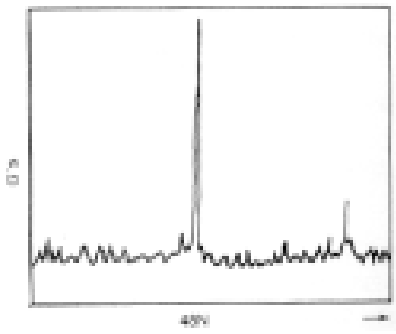

Fig. 31. High-Pressure Bleed Chamber - 5,400 rpm

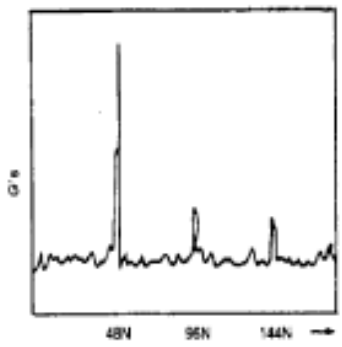

Fig. 32. High-Pressure Bleed Chamber - 8,000 rpm

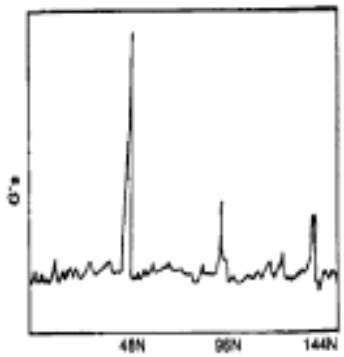

Fig. 33. High-Pressure Bleed Chamber - 9,400 rpm

Next, the fifth-stage pressure was measured. Once again, high amplitude at 48*N* was found. However, a predominant reading was also observed at 1,200 Hz frequencies. Figures 34 and 35 shows the largest amplitudes at speeds of 5,800 and 6,800 rpm, respectively.

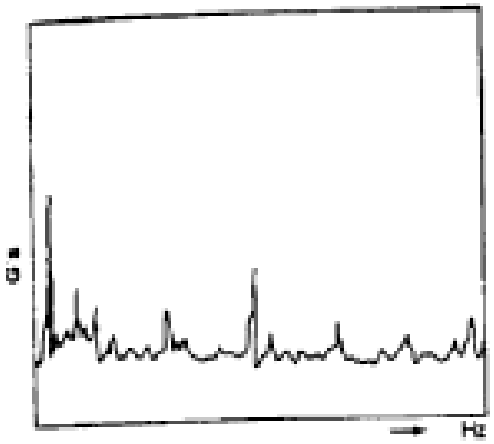

Fig. 34. Fifth Stage Bleed Pressure - 5800 rpm

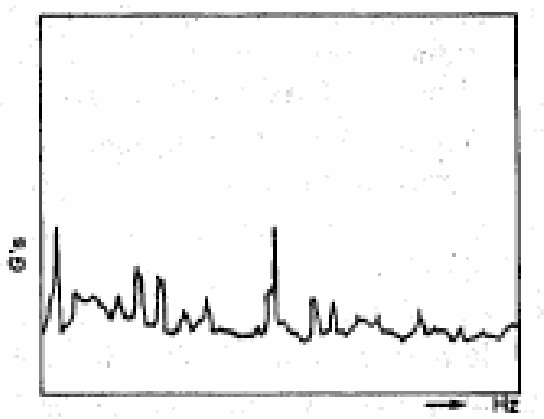

Fig. 35.Fifth-Stage Bleed Pressure - 6,800 rpm

At the compressor exit, predominate frequencies of 48*N* existed up to speeds of 6,800 rpm. At 8,400 rpm, the 48*N* and 86*N* frequencies were of about equal magnitudes - the only signal where the 48*N* and 86*N* frequencies were the same. The pressure was measured from a static port in the chamber. All other pressures were measured from the shroud, thus indicating the phenomena occurred at the blade tip. Since the problem was isolated to the fifth stage, the conclusion was that the stall occurred at the fifth-stage rotor tip. The solution to the problem was the redesign of the fifth stage blade with a modified angle so that it would not be as subject to stall flutter.

2.0-10 Compressor Performance Parameters

For a gas compressor, the functional dependence of compressor exit total/stagnation pressure P_{texit} and the adiabatic compressor efficiency η_c can be expressed as follows:

$$(P_{texit}, \eta_c) = F(\dot{m}, P_{tin}, T_{tin}, N, \nu, R, \gamma, \text{design } D) \quad . \tag{29}$$

The gas properties of relevance to the compression process are characterized by the kinematic viscosity ν, specific heat ratio γ, and the gas constant R. The geometry dependence of the machine is set by the design and its characteristic size D such as the tip diameter of compressor. Use of dimensional analysis reduces the complexity of Equation (29) (noting that γ and design D, can be regarded as non-dimensional) to yield

$$\frac{P_{texit}}{P_{tin}}, \eta_c = F\left(\frac{\dot{m}\sqrt{RT_{tin}}}{P_{tin}D^2}, \frac{ND}{\sqrt{\gamma RT_{tin}}}, \frac{ND^2}{\nu}, \gamma\right), \tag{30}$$

For a given compressor and for inlet conditions for which γ does not vary, Equation (30) reduces to

$$\frac{P_{texit}}{P_{tin}}, \eta_c = F\left(\frac{\dot{m}\sqrt{T_{tin}}}{P_{tin}}, \frac{N}{\sqrt{T_{tin}}}, \frac{ND^2}{\nu}\right), \tag{31}$$

At high enough Reynolds number (> 3 x 10^5), changes in this number have little effect on compressor performance so that

$\left(\frac{P_{texit}}{P_{tin}}, \eta_c\right)$ can be correlated in terms of $\left(\frac{\dot{m}\sqrt{T_{tin}}}{P_{tin}}, \frac{N}{\sqrt{T_{tin}}}\right)$ i.e.

$$\frac{P_{texit}}{P_{tin}}, \eta_c = F\left(\frac{\dot{m}\sqrt{T_{tin}}}{P_{tin}}, \frac{N}{\sqrt{T_{tin}}}\right) \tag{32a}$$

As no functional dependence is implied if the non-dimensional variables on the right hand side is scaled by a constant, one can thus choose to replace them by the corrected mass flow rate $\dot{m}_c = \left(\frac{\dot{m}\sqrt{\theta}}{\delta}\right)$ and corrected speed $N_c = \left(\frac{N}{\sqrt{\theta}}\right)$ so that

$$\frac{P_{texit}}{P_{tin}}, \eta_c = F\left(\frac{\dot{m}\sqrt{\theta}}{\delta}, \frac{N}{\sqrt{\theta}}\right) = \mathrm{F}(\dot{m}_c, N_c). \tag{32b}$$

In equation (32b), $\theta = \frac{T_{tin}}{T_{ref}}$ and $\delta = \frac{P_{tin}}{P_{ref}}$ where the reference temperature T_{ref} and the reference pressure P_{ref} are taken to be the sea-level value for the standard atmosphere, 59.6ºF (15°C) and 14.7 psia (101 KN/m²) respectively. The advantage of using these corrected variables is that their numerical magnitude is similar to the actual value so that its significance is not obscured.

We can also use the Euler Turbine Equation (8) for a compressor stage

$$\mathrm{c_p}\,(\mathrm{T_{texit}} - \mathrm{T_{tin}}) = \omega\left[(\mathrm{rV_\theta})_2 - (\mathrm{rV_\theta})_1\right] \tag{33}$$

to elucidate the functional dependence and to deduce why the performance characteristics look the way they are on a compressor map. Assuming isentropic flow (i.e. no loss) then the stagnation pressure ratio across the (ideal) stage is given by

$$PR_s = \frac{p_{texit}}{p_{tin}} = \left\{1 + \left[\frac{(\omega r_2)^2}{c_p T_{tin}}\right]\left[1 - \left(\frac{V_{z2}}{\omega r_2}\right)\left(\tan\beta_{exit} + \frac{V_{z1}r_1}{V_{z2}r_2}\tan\alpha_{exit}\right)\right]\right\}^{\frac{\gamma}{\gamma-1}} \tag{34}$$

In equation (33) and (34) subscript 1 and 2 refer to variable evaluated at rotor inlet and rotor exit respectively, V_θ denotes tangential velocity, V_z the axial velocity, ω the angular velocity of rotor, α_{exit} the absolute flow angle at stator exit, β_{exit} the relative flow angle at rotor exit, and r the radius. Upon introducing the corrected variables into equation (34) we have

$$R_s = \left\{1 + k_0 N_c^2 - k_1 N_c \dot{m}_c G(M_1)(\tan\alpha_{exit} + \tan\beta_{exit})\right\}^{\frac{\gamma}{\gamma-1}} \tag{35}$$

where $G(M_1)$ has a weak dependence on the incoming Mach number M_1, $k_0 \propto r^2$ and $k_1 \propto r$. For a given compressor stage $(\tan\alpha_{exit} + \tan\beta_{exit})$ is fixed and neglecting the variation in $G(M_1)$ we have $PR_s = PR_s(\dot{m}_c, N_c)$. The general dependence of PR_s on $\dot{m}_c$ and N_c is shown in figure 39 as a series of dashed lines of constant corrected speed for the ideal stage; equation (35) can be used to obtain the trend in the variation of the ideal stage characteristic with $\dot{m}_c$ and N_c. The solid lines (of constant corrected speed) in figure 36 are the PR_s vs $\dot{m}_c$ curves with stagnation pressure losses taken into account. Flow angle varies as corrected mass flow rate changes along a given corrected speed line. The point of minimum difference between the dash (ideal) and the solid (actual) curve corresponds to a corrected mass flow that yields an angle of incidence for minimum loss; moving away from this point along a constant corrected speed line amounts to changing the incidence angle (increasing the angle of incidence for decreasing $\dot{m}_c$ or decreasing the angle of incidence for increasing $\dot{m}_c$) so as to lead to higher loss. This is reflected in the increasing difference between the two curves (ideal versus actual) at corrected mass flow other than that corresponding to minimum loss. One thus deduces from the above arguments that the actual pressure rise (and the efficiency) can also be characterized in terms of $\dot{m}_c$ and N_c. The pressure ratio of a complete compressor consisting of many stages can be obtained by taking the products of the stage performance.

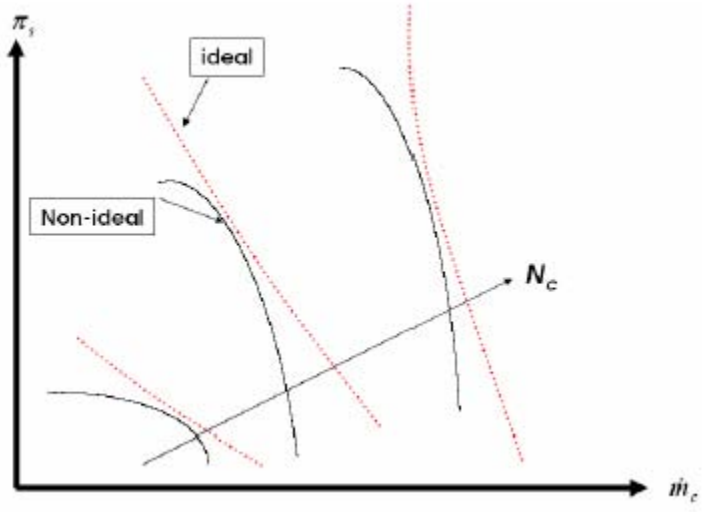

Fig. 36. Performance map of compressor stage

2.0-11 Performance Losses in an Axial-Flow Compressor

The calculation of the performance of an axial-flow compressor at both design and off-design conditions requires the knowledge of the various types of losses encountered in an axial-flow compressor.

The accurate calculation and proper evaluation of the losses within the axial-flow compressor are as important as the calculation of the blade-loading parameter, since unless the proper parameters are controlled, the efficiency drops. The evaluation of the various losses is a combination of experimental results and theory. The losses are divided into two groups: (1) losses encountered in the rotor, and (2) losses encountered into the stator. The losses are usually expressed as a loss of heat and enthalpy.

A convenient way to express the losses is in a nondimensional manner with reference to the blade speed. The theoretical total head available (q_{tot}) is equal to the head available from the energy equation ($q_{th} = q_{tot}$) plus the head which is loss from disc friction.

$$q_{tot} = q_{th} + q_{fl} \tag{36}$$

The adiabatic head that is actually available at the rotor discharge is equal to the theoretical head minus the heat losses from the shock in the rotor, the incidence loss, the blade loadings and profile losses, the clearance between the rotor and the shroud, and the secondary losses encountered in the flow passage

$$q_{ia} = q_{th} - q_{in} - q_{sh} - q_{bl} - q_{cl} - q_{sf} \ . \tag{37}$$

Therefore, the adiabatic efficiency in the impeller is

$$\eta_{imp} = \frac{q_{ia}}{q_{tot}} \ . \tag{38}$$

The calculation of the overall stage efficiency must also include the losses encountered in the stator. Thus, the overall actual adiabatic head attained would be the actual adiabatic head of the impeller minus the head losses encountered in the stator from wake caused by the impeller blade, the loss of part of the kinetic head at the exit of the stator, and the loss of head from the frictional forces encountered in the stator

$$q_{a} = q_{ii} - q_{w} - q_{k} - q_{osf} \quad . \tag{39}$$

Therefore, the adiabatic efficiency in the stage

$$\eta stage = \frac{q_{a}}{q_{tot}} \quad . \tag{40}$$

The losses as mentioned earlier can be further described:

1. *Disc friction loss.* This loss is from skin friction on the discs that house the blades of the compressors. This loss varies with different types of discs.
2. *Incidence loss.* This loss is caused by the angle of the air and the blade angle not being coincident. The loss is at a minimum to about an angle of ± 4°, after which the loss increases rapidly.
3. *Blade loading and profile loss.* This loss is due to the negative velocity gradients in the boundary layer, which gives rise to flow separation.
4. *Skin friction loss.* This loss is from skin friction on the blade surfaces and on the annular walls.
5. *Clearance loss.* This loss is due to the clearance between the blade tips and the casing.
6. *Wake loss.* This loss is from the wake produced at the exit of the rotary.
7. *Stator profile and skin friction loss.* This loss is from skin friction and the attack angle of the flow entering the stator.
8. *Exit loss.* This loss is due to the kinetic energy head leaving the stator.

Figure 37 shows the various losses as a function of flow. Note that the compressor is more efficient as the flow nears surge conditions.

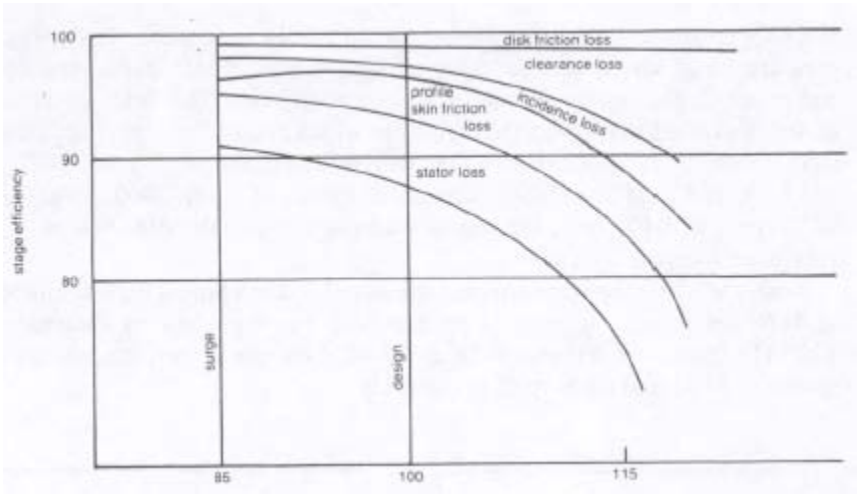

Fig. 37. Losses in an axial-flow compressor stage

2.0-12 New Developments in Axial Flow Compressors

The new advanced compressor rotors have fewer blades with higher loadings, and the blades are thinner, larger, and are designed using advanced radial equilibrium theory, which create Three Dimensional and Controlled Diffusion shaped airfoils (3D/CDA), with smaller clearances and higher loading per stage.

There are also trends towards water injection at the inlet or between compressor sections which will likely affect airfoil erosion life. The smaller clearances (20-50 mils) and high pressure ratios tend to increase the probability of encountering rubs. These tip rubs usually occur near the bleed flow sections of the turbines where there are inner diameter changes and the compressor casing could be out of round. Figure 38 shows one such blade that encountered tip rub.

Fig. 38. Compressor Blade with Tip Rub

The advanced compressor blades also usually have squealer sections on the blade tips, which are designed to wear in a safe manner if the blades are in contact with the casing. Figure 39 is one such blade. These rubs, if severe can lead to tip fractures and overall destruction of the downstream blades and diffuser vanes due to domestic object damage (DOD).

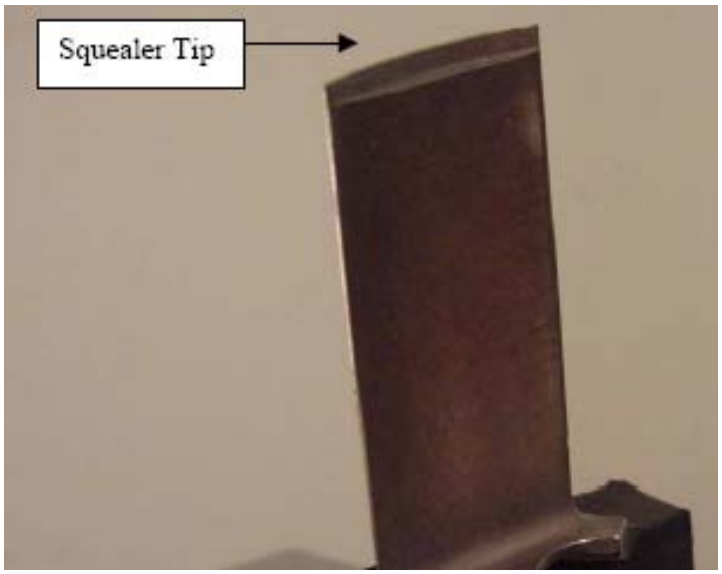

Fig. 39. Axial Flow Compressor rotor blade with squealer tip

The very high temperature at the exit of the compressor, which in some cases exceeds a 1000ºF, causes a very hot compression section, which also requires the cooling of the bleed flows before they can be used for cooling the turbine section. This requires large heat exchangers and in some combined cycle plants steam is used to cool the compressed air. This also limits the down time between start-ups of the turbines. Design margins are set by Finite Element Modeling (FEM) at the element level which results in lower safety margins than previous designs. The costs of these larger, thinner, less-rub tolerant, and more twisted-shape airfoils are usually higher. When several of the major characteristics of advanced gas turbines are examined from a risk viewpoint (i.e., probability and consequences of failure), there are no characteristics which reduce the probability of failure and/or decrease the consequence of failure.

Table 3 indicates the changes in the compressor blades that are now prevalent on the advanced gas turbines. The first column represents previous gas turbine designs, the second column represents new gas turbine designs, and the last column indicates the change in risk (⬆ represents higher) for the design differences. Most of the comparisons are self-explanatory.

Table 3 State of Gas Turbine Technology Compressors

Previous Designs	**New Designs**	**Risk**
• 2D double circular arc or NACA 65 profiles	• 3D or Controlled Diffusion Airfoil (CDA) profiles	⬆
• Large number of airfoils	• Reduced airfoil count	⬆
• Repeating stages/shorter chords	• Stages unique/longer chords	⬆
• Low/ modest Aspect ratios	• High Aspect ratios	⬆
• Large clearances	• Smaller clearances	⬆
• Low/modest pressure ratios (R_c)	• Much higher pressure ratios (R_c)	⬆
• Low/modest blade loading per stage	• High blade loading per stage	⬆
• Wider Operating margin	• Narrow operating margin	⬆
• Thicker leading edges	• Thinner leading edges	⬆
• Dry operation	• Wet operation	⬆
• Bulk safety margins	• Safety margins by FEM	⬆
• Lower costs	• Higher costs	⬆

2.0-13 Recent Advances and Research Requirements

There is considerable research is being carried out on improving the performance of axial flow compressor. This research is being carried out in many different aspects of the axial flow compressor:

1. Effects of Aspect Ratio on blade loading, blade excitation, and the pre-twist blade angles (centrifugal forces on the blade). Increase in blade loading was carried out by increasing the Aspect ratio of the blade. Blade aspect ratios were increased to AR = 9. At these high aspect ratios the blades had to be designed with mid span shrouds, and tip shrouds. This decreases the efficiency of the stage; however, without the shrouds the pre-twist blade angle had to be increased to about 12º, and the blade excitation resulted in blade failure. Presently most blade designs are limited to an AR=4.

2. Increasing the operational range (surge – choke) at a given compressor speed, by developing new blade profiles to reduce blade stall in compressors

   Cascade Tests

   The data on blades in an axial-flow compressor are from various types of cascades, since theoretical solutions are very complex, and their accuracy is in question because of the many assumptions required to solve the equations. The most thorough and systematic cascade testing has been conducted by NACA staff at the Lewis Research Center. The bulk of the cascade testing was carried out at low mach numbers and at low turbulence levels.

   The NACA 65 blade profiles were tested in a systematic manner by Herrig, Emergy, and Erwin. The cascade tests were carried out in a cascade wind tunnel with boundary-layer suction at the end walls. Tip effects were studied in a specially designed water cascade tunnel with relative motion between wall and blades.

   Cascade tests are useful in determining all aspects of secondary flow. For better visualization, tests have been conducted in water cascades. The flow patterns are studied by injecting globules of dibutyl phatalate and kerosene in a mixture equal to the density of water. The mixture is useful in tracing secondary flow, since it does not coagulate.

   An impeller designed for air can be tested using water if the dimensionless parameters, Reynolds number (R_e), and specific speed (N_s) are held constant

$$R_e = \frac{\rho_{air} V_{air} D}{\mu_{air}} = \frac{\rho_{water} V_{water} D}{\mu_{water}} \quad (41)$$

$$N_s = \frac{Q_{air}}{N_{air} D^3} = \frac{Q_{water}}{N_{water} D^3} \tag{42}$$

where:

ρ = medium density
V = velocity
D = impeller diameter
μ = viscosity
N = speed

Using this assumption, one can apply this flow visualization method to any working medium.

One designed apparatus consists of two large tanks on two different levels. The lower tank is constructed entirely out of Plexiglas and receives a constant flow from the upper tank. The flow entering the lower tank comes through a large, rectangular opening which houses a number of screens so that no turbulence is created by water entering the lower tank. The center of the lower tank can be fitted with various boxes for the various flow visualization problems to be studied. This modular design enables a rapid interchanging of models and work on more than one concept at a time.

Blade Profile

To study the effect of laminar flow, the blades were slotted as shown in figure 40. For the blade treatment cascade rig experiment, a Plexiglas cascade was designed and built. Figure 41 shows the cascade. This cascade was then placed in the bottom tank and maintained at a constant head. Figure 42 shows the entire setup, and figure 43 shows the cascade flow. Note the large extent of the laminar-flow regions on the treated center blades as compared to the untreated blades.

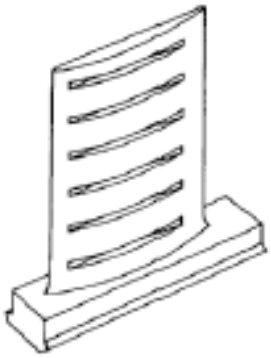

Fig. 40. Perspective of compressor blade with treatment

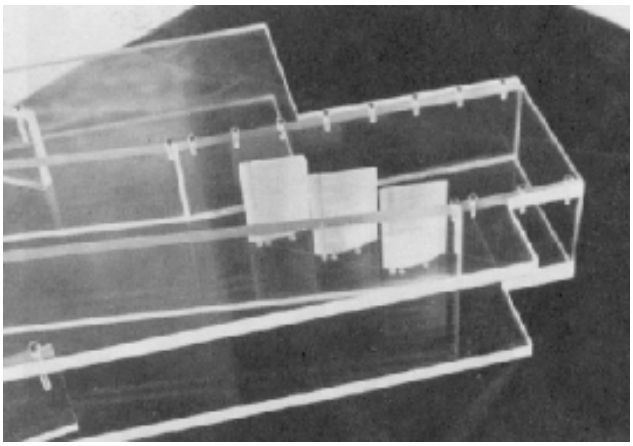

Fig. 41. Cascade model in axial-flow test tank

Fig. 42. Apparatus for testing axial-flow cascade model

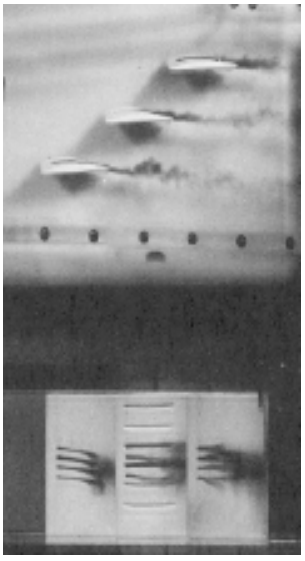

Fig. 43. Treatments on center cascade blade

3. Reduction of flow leakage at the compressor tips

The effect of casing treatment in axial-flow compressors was studied in a water cascade tunnel. In this study the same Reynold number and specific speeds were maintained as those experienced in an actual axial-flow compressor.

In an actual compressor the blade and the passage are rotating with respect to the stationary shroud. It would be difficult for a stationary observer to obtain data on the rotating blade passage. However, if that observer were rotating with the blade passage, data would be easier to acquire. This was accomplished by holding the blade passage stationary with respect to the observer and rotating the shroud. Furthermore, since casing treatment affects the region around the blade tip, it was sufficient to study only the upper portion of the blade passage. These were the criteria in the design of the apparatus.

The modeling of the blade passage required provisions for controlling the flow in and out of the passage. This control was accomplished by placing the blades, which partially form the blade passage, within a Plexiglas tube. The tube had to be of sufficient diameter to accommodate the required flow through the passage without tube wall effect distorting the flow as it entered or left the blade passage. This allowance was accomplished by using a tube three times the diameter of the blade pitch. The entrance to the blades was designed so that the flow entering the blades was a fully developed turbulent flow. The flow in the passage between the blade tip and the rotating shroud was laminar. This laminar flow was expected in the narrow passage.

A number of blade shapes could have been chosen; therefore, it was necessary to pick one shape for this study, which would be the most representative for casing treatment considerations. Since casing treatment is most effective from an acoustic standpoint in the initial stages of compression, the maximum point of camber was chosen toward the rear of the blade (Z = .6 chord). This type of blade profile is most commonly used for transonic flow and is usually in the initial stages of compression.

The rotating shroud must be in close proximity to the blade tips within the tube. To get this proximity, a shaft-mounted Plexiglas disc was suspended from above the blades. The Plexiglas disc was machined as shown in figure 44. The Plexiglas tube was slotted so that the disc could be centered on the centerline of the tube and its stepped section lowered through the two slots in the tube. Clearances between the slot edges and the disc were minimized. One slot was cut directly above the blade passage emplacement. The other slot was sealed off to prevent leakage. As the disc was lowered into close proximity to the blade tips, the blade passage was completed. The clearance between disc and blade was kept at 0.035 of an inch. The disc, when spun from above, acted as the rotating shroud.

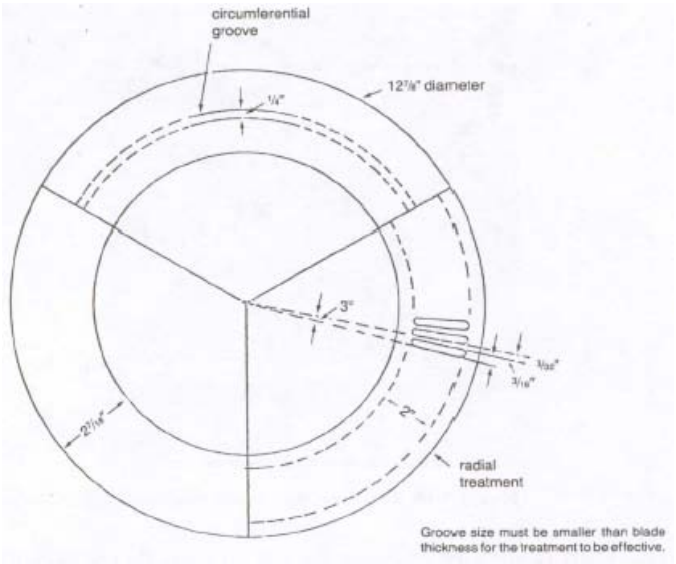

Fig. 44. Details of the various casing treatments. (Each treatment was on a separate disc)

There are only two basic casing treatment designs other than a blank design - which corresponds to no casing treatment at all. The first type of casing treatment consists of radial grooves. A radial groove is a casing treatment design in which the groove is essentially parallel to the chordline of the blade. The second basic type is the circumferential groove. This type of casing treatment has its grooves perpendicular to the blade chordline. Figure 45 is a photograph of two discs showing the two types of casing treatment used. The third disc used is a blank, representing the present type of casing. The results indicate that the radial casing treatment is most effective in reducing leakage and also in increasing the surge-to-stall margin. Figure 46 shows the leakage at the tips for the various casing treatments. Figure 47 shows the velocity patterns observed by the use of various casing treatments. Note that for the treatment along the chord (radial), the flow is maximized at the tip. This flow maximum at the tip indicates that the chance of rotor tip stall is greatly reduced.

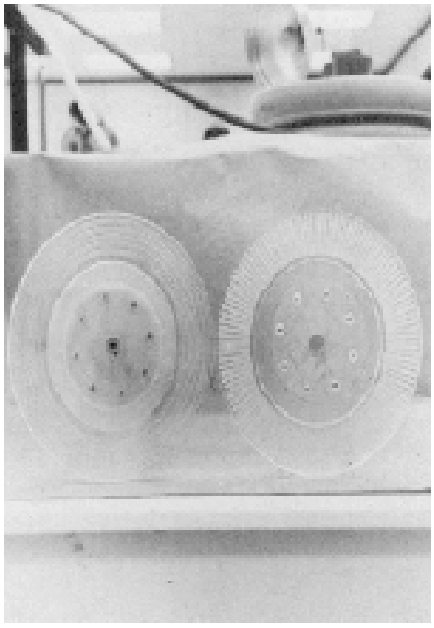

Fig. 45. Two discs with casing treatment

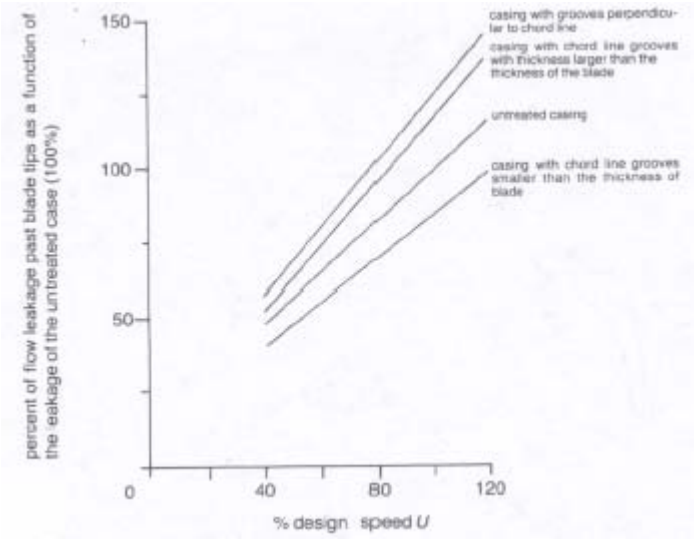

Fig. 46. Mass flow leakage at tips for various casing treatments

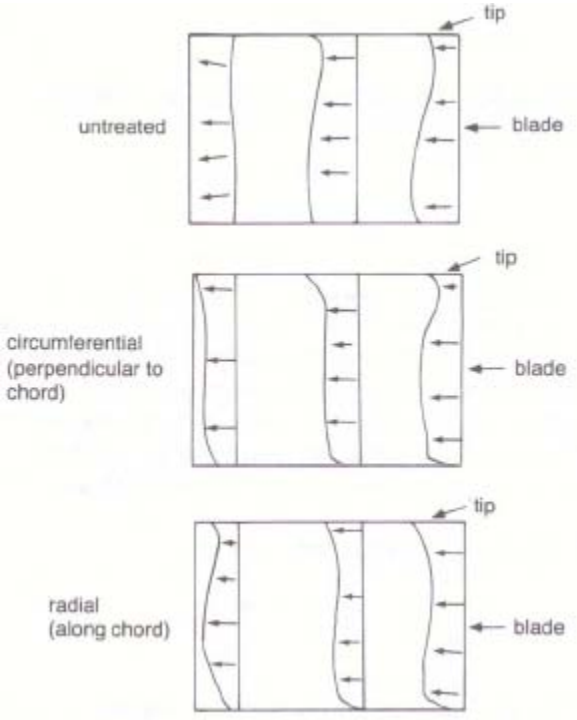

Fig. 47. Velocity patterns observed in the side view of the blade passage for various casing treatments

4. Enhancement of Numerical Solutions of the Navier-Stokes Equation (viscous compressible flow)

The solution of the full Navier Stokes equation requires much enhanced numerical techniques. The old solutions used inviscous flow and quasi three dimensional flow solutions. There are many new enhanced numerical programs underway to solve the equation in its entirety.

5. Supersonic Blade Profiles for higher pressure ratio per stage (>2.1)

Transonic blades have been designed with the point of maximum thickness at about 0.6 of blade chord from the leading edge of the blade. Supersonic blade design has problems with standing shock waves which can occur as the flow enters the stators. The losses with the diffusion process is very high and thus design changes are being tested so that the flow entering the diffuser is easily swallowed, and that if any shock waves exist they are oblique shocks with minimal losses. Cascade testing is being conducted on various profiles to ensure that the stage losses are minimized.

6. Compressor interstage cooling by water injection between stages

In this system the water is injected into the mid-stages of the compressor to cool the air and approach an isothermal compression process as shown in figure 48. The water injected is usually mechanically atomized so that very fine droplets are entered into the air. The water is evaporated as it comes in contact with the high pressure and temperature air stream. As water evaporates, it consumes about 1058 BTU (1117 kJ) (latent heat of vaporization) at the higher pressure and temperature resulting in lowering the temperature of the air stream entering the next stage. This lowers the work required to drive the compressor. The intercooling of the compressed air has been very successful when applied to high-pressure ratio engines.

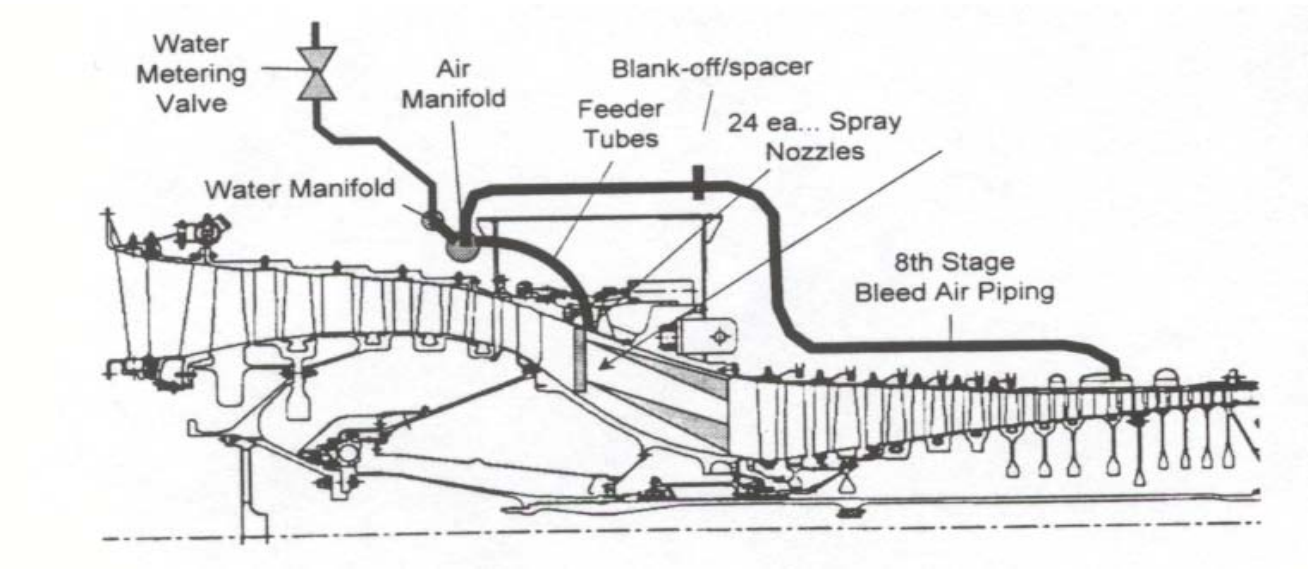

Fig. 48. Mid-Compressor Cooling showing a schematic as well as an actual application in a GE LM 6000 Engine (courtesy GE Power Systems)

2.0-14 Compressor Blade Material

Compressor blading is made by forging, extrusion or machining. All production blades, until the advent of he new Advanced Gas Turbines, have been made from stainless steels, Type 403 or 403 Cb both having about 12 Cr. This family of alloys has properties which include good ductility at high strength levels, uniform properties, and good strength at temperatures up to about 900ºF (482ºC). Because of the new axial flow compressors which have pressure ratio of 30:1 to 40:1, and exit temperatures between 1000ºF – 1150ºF (538ºC - 621ºC), new compressor blade material, a precipitation hardened, martensitic stainless steel such as 15-5 PH nominal, was introduced into production for advanced and uprated machines, as shown in Table 4. This material provides increased tensile strength without sacrificing stress corrosion resistance. Substantial increases in the high-cycle fatigue and corrosion fatigue strength are also achieved with this material, compared with the Type 403 stainless steel with 12Cr. Superior corrosion resistance is also achieved due to the metal's higher concentration of chromium and molybdenum content. Compressor corrosion results from moisture containing salts and acids collecting on the blading. During operation, moisture can be present because of rain, use of evaporative coolers, fogging systems, or compressor water washes, or condensation resulting from humid air being accelerated at the compressor inlet. Moisture may be present in the compressor during operation up to between stage 5 and stage 8, where it usually becomes warm enough to prevent condensation. When the turbine is not in operation, the compressor can still become wet if metal temperatures are below the local dew point. This can happen to units stored in humid environments. The chemistry of this moisture deposit, especially the salt in the air depositing on the blading, determines the severity of the corrosion phenomenon.

Table 4 Compressor Blade Material

Compressor Blade Type	Max. Temp	COMPONENTS PERCENT													
		C	S	Mn	P	Si	Cr	Mo	Ni	Cu	Al	Cb	Mg	O	Fe
AISI 403	900ºF	.11					12						-	-	Bal
AISI 403+Cb	900ºF	.15	-	-	-	-	12	-	-	-	-	0.2	-	-	Bal
Martensitic High Temperature Stainless Steel	1250ºF	.08	-	.14	-	.4	15.6	.08	3.8-6.5	2.9	.9	-	-	-	Bal
15-5 PH, nominal		<.07	<.03	<1.0	<0.04-	<1.0	14-15.5	-	3.5-5.5	3.2	.9	.15-.45	-	-	Bal

The high temperature blade alloy is normally produced by vacuum-arc remelting to reduce inclusions, and is advertised to have a balanced chemistry that minimizes the formation of delta-ferrite. Inclusions and the delta-ferrite would provide planes of weakness in that part. It is not uncommon for the mill to supply forging stock that has first been given a 1900ºF heat treatment, just for better forgeability. The forged blanks are then usually reheat-treated at 1900ºF, followed by hardeningtreatments between 1100ºF and 1150ºF depending on the properties sought. There is a general correlation between hardness and strength (tensile/fatigue). A hardness of RC 32 suggests that the tensile strength is around 150000 psi and that the hardening temperature used during manufacture was somewhere around 1100ºF to 1150ºF.

Coating of the compressor blades is now very common. Compressor blades suffer a great amount of corrosion pitting from impurities in the air stream. This corrosion pitting has led to blade failures. Compressor blades in many cases have over 100,000 hours but due to pitting can be reduced considerably to between 20,000 – 60,000 hours. It has been a very common practice for over 30 years to coat at least the first 5-8 stages depending on the compressor design. The first stages are considered to be the "wet stages" because many units now use on line water washes, as well as have evaporative cooling and fogging for power augmentation.

Coating for these blades is usually consistent of a duplex type coating, which must be at least 3 mils in thickness. This coating as most typical coating has a sacrificial undercoat coating which is placed on the base metal and is covered by a ceramic coating. Ni-Cd coating is also used in selected applications, and new coatings consisting of an aluminum slurry coating which has a protective ceramic top layer that provides improved erosion resistance are also being introduced. This type of coating, as compared to conventional aluminum slurry coatings, is better in corrosion protection and substantially better in erosion resistance. This type of coating also improves the performance of the gas turbine by reducing the amount of power consumed by the compressor. Tests conducted show a reduction of 2%-3% in the power consumed by the compressor which pays back additional cost of coating in 4-6 months of operation.

The aspect ratio of axial flow compressors including the IGV vary from about AR = 4, to an aspect ratio of about AR = 0.5. All IGV's and the first five to eight stages of rotating and stationary airfoils in the compressor are made from Martensitic High Temperature Stainless Steel; or 15-5 PH nominal blade material, the next stages are usually coated AISI 403 or 403 Cb.

2.0-15 Acknowledgements

This chapter has been taken liberally from the author's book *Gas Turbine Engineering Handbook*. The author would like to express his sincere thanks to Dr. Choon Sooi Tan and Dr. Yifang Gong for their contributions to the sections on Stall Flutter, and Compressor Performance Parameters. Dr. Tan is a senior research engineer, and Dr. Gong is a research engineer at the MIT Gas Turbine Laboratory.

Dr. Tan is a leading authority on unsteady and three dimensional flow in multistage Turbomachinery and is an author of 38 publications and a co-author of the book entitled, *Internal Flow: Concepts and Applications,* Cambridge University Press, 2004.

Dr Gong is an authority on compressor aerodynamics and instability in compressor/compression systems; he is presently working on the design and development of a gas turbine power plant using supercritical CO_2 as the working fluid.

2.0-16 Bibliography

1. Boyce, M.P,, Gas Turbine Engineering Handbook, Second Edition, Butterworth-Hienemann 2003
2. Herrig, L.J., Emery, J.C., and Erwin, J.R., "Systematic Two Dimensional Cascade Tests of NACA 65 Series Compressor Blades
   at Low Speed," NACA R.M. E 55H11 (1955).
3. Boyce, M.P., "Fluid Flow Phenomena in Dusty Air," (Thesis), University of Oklahoma Graduate College, 1969, p. 18.
4. Boyce M.P., Schiller, R.N., and Desai, A.R., "Study of Casing Treatment Effects in Axial-Flow Compressors," ASME Paper No. 74-GT-89.
5. Boyce, M.P., "Secondary Flows in Axial-Flow Compressors with Treated Blades," AGARD-CCP-214 pp. 5-1 to 5-13.
6. Giamati, C.C., and Finger, H.B., "Design Velocity Distribution in Meridional Plane," NASA SP 36, Chapter VIII (1965), p. 255.
7. Hatch, J.E., Giamatic, C.C., and Jackson, R.J. "Application of Radial Equilibrium Condition to Axial-Flow Turbomachine Design Including Consideration of Change of Enthropy with Radius Downstream of Blade Row," NACA RM E54A20 (1954)
8. Holmquist, L.O., and Rannie, W.D., "An Approximate Method of Calculating Three-Dimensional Flow in Axial Turbomachines" (Paper) Meeting Inst. Aero. Sci., New York, January 24-28, 1955.
9. Lieblein, S., Schwenk, F.C., and Broderick, R.L., "Diffusion Factor for Estimating Losses and Limiting Blade Loading in Axial-Flow Compressor Blade Elements," NACA RM #53001 (1953).
10. Stewart, W.L., "Investigation of Compressible Flow Mixing Losses Obtained Downstream of a Blade Row," NACA RM E54120 (1954).
11. Boyce, M.P., "Transonic Axial-Flow Compressor." ASME Paper No. 67-GT-47.
12. Carter, A.D.S., "The Low-Speed Performance of Related Aerofoils in Cascade," Rep. R.55, British NGTE, September, 1949.
13. Mellor, G., "The aerodynamic Performance of Axial Compressor Cascades with Applications to Machine Design," (Sc. D. Thesis), M.I.T. Gas Turbine Lab, M.I.T. Rep. No. 38 (1957).
14. Graham, R.W. and Guentert, E.C., "Compressor Stall and Blade Vibration," NASA SP 365, (1956) Chapter XI, p.311.
15. Cumpsty, N. A., 1989, *Compressor Aerodynamics*, Longman Group UK Ltd., London, England.
16. Cumpsty, N. A., 1998, *Jet Propulsion*, Cambridge University Press, Cambridge, England.
17. Hill, P. G., Peterson, C. R., 1992, *Mechanics and Thermodynamics of Propulsion*, Second Edition, Addison-Wesley Publishing Company, Reading MA.
18. Kerrebrock, J. L., 1992, *Aircraft Engines and Gas Turbines*, MIT Press, Cambridge, MA.
19. Khalak, A., 2002, "A Famework for Futter Clearance of Aeroengine Blades", Journal of Engineering for Gas Turbine and Power, Vol 124, No. 4. Also ASME 2001-GT-0270, ASME Turbo Expo 2001, New Orleans, LA, 2001.
20. Mikolajczak, A. A., Arnoldi, R. A., Snyder, L.E., Stargardter, 1975, "Advances in Fan and Compressor Blade Flutter Analysis and Prediction," Journal of Aircraft 12.
21. Caltech Lecture Notes on Jet Propulsion JP121 Graduate Course (Instructor: Zukoski E. E.)

BIOGRAPHY

2.0 Axial-Flow Compressors

Meherwan P. Boyce

2121 Kirby Drive, Number 28N
Houston, TX 77019

phone: (713) 807--0888
fax: (713) 807-0088
email: mpboyce@boycepower.com
boycepower.com

Dr. Meherwan P. Boyce, P.E., Fellow ASME & IDGTE; has over 42 years of experience in the field of TurboMachinery in both industry and academia. His industrial experience covers 20 years as Chairman and CEO of Boyce Engineering International, and five years as a designer of compressors and turbines for gas turbines for various gas turbine manufacturers. His academic experience covers a 15 year period, which includes the position of Professor of Mechanical Engineering at Texas A&M University and Founder of the TurboMachinery Laboratories and The TurboMachinery Symposium, which is now in its thirtieth year. He is the author of several books such as the Gas Turbine Engineering Handbook (Butterworth & Heinemann), Cogeneration & Combined Cycle Power Plants (ASME Press), and Centrifugal Compressors, A Basic Guide (PennWell Books). He is a contributor to several Handbooks; his latest contribution is to the Perry's Chemical Engineering Handbook Seventh Edition (McGraw Hill) in the areas of Transport and Storage of Fluids, and Gas Turbines. Dr. Boyce has taught over 100 short courses around the world attended by over 3000 students representing over 400 Companies. He is a Consultant to the Aerospace, Petrochemical and Utility Industries globally, and is a much-requested speaker at Universities and Conferences throughout the world.

Dr. Boyce is Chairman of the Plant Engineering & Maintenance Division of ASME, and Chairman of the Electric Utilities Committee of the of ASME's International Gas Turbine Institute. He is also a Chairman of the ASME Conferences Committee. In 2002 Dr Boyce was chairman of two major conferences the Advanced Gas Turbine and Condition Monitoring Conference sponsored by DOE and EPRI, and the Gas Turbine Users Associations Conference.

Dr. Boyce has authored more than 100 technical papers and reports on Gas Turbines, Compressors Pumps, Fluid mechanics, and TurboMachinery. He is a Fellow of the ASME (USA) and the Institution of Diesel and Gas Turbine Engineers (UK), and member of SAE, NSPE, and several other professional and honorary societies such as Sigma Xi, Pi Tau Sigma, Phi Kappa Phi, and Tau Beta Phi. He is the recipient of the ASME award for Excellence in Aerodynamics and the Ralph Teetor Award of SAE for enhancement in Research and Teaching He is also a Registered Professional Engineer in the State of Texas.

Dr. Boyce received a B.S. and M.S. in Mechanical Engineering from the South Dakota School of Mines and Technology and the State University of New York, respectively, and Ph.D. in Aerospace & Mechanical Engineering in 1969 from the University of Oklahoma.